A TRIPLE-POROSITY MODEL FOR FRACTURED HORIZONTAL WELLS

A Thesis

by

HASAN ALI H ALAHMADI

Submitted to the Office of Graduate Studies of
Texas A&M University
in partial fulfillment of the requirements for the degree of

MASTER OF SCIENCE

August 2010

Major Subject: Petroleum Engineering

A Triple-Porosity Model for Fractured Horizontal Wells

A TRIPLE-POROSITY MODEL FOR FRACTURED HORIZONTAL WELLS

A Thesis

by

HASAN ALI H ALAHMADI

Submitted to the Office of Graduate Studies of
Texas A&M University
in partial fulfillment of the requirements for the degree of

MASTER OF SCIENCE

Approved by:

Chair of Committee,	Robert A. Wattenbarger
Committee Members,	J. Bryan Maggard
	William Rundell
Head of Department,	Stephen A. Holditch

August 2010

Major Subject: Petroleum Engineering

ABSTRACT

A Triple-Porosity Model for Fractured Horizontal Wells. (August 2010)

Hasan Ali H Alahmadi, B.Sc., King Fahd University of Petroleum and Minerals

Chair of Advisory Committee: Dr. Robert A. Wattenbarger

Fractured reservoirs have been traditionally idealized using dual-porosity models. In these models, all matrix and fractures systems have identical properties. However, it is not uncommon for naturally fractured reservoirs to have orthogonal fractures with different properties. In addition, for hydraulically fractured reservoirs that have pre-existing natural fractures such as shale gas reservoirs, it is almost certain that these types of fractures are present. Therefore, a triple-porosity (dual-fracture) model is developed in this work for characterizing fractured reservoirs with different fractures properties.

The model consists of three contiguous porous media: the matrix, less permeable micro-fractures and more permeable macro-fractures. Only the macro-fractures produce to the well while they are fed by the micro-fractures only. Consequently, the matrix feeds the micro-fractures only. Therefore, the flow is sequential from one medium to the other.

Four sub-models are derived based on the interporosity flow assumption between adjacent media, i.e., pseudosteady state or transient flow assumption. These are fully transient flow model (Model 1), fully pseudosteady state flow model (Model 4) and two mixed flow models (Model 2 and 3).

The solutions were mainly derived for linear flow which makes this model the first triple-porosity model for linear reservoirs. In addition, the Laplace domain solutions are also new and have not been presented in the literature before in this form.

Model 1 is used to analyze fractured shale gas horizontal wells. Non-linear regression using least absolute value method is used to match field data, mainly gas rate. Once a match is achieved, the well model is completely described. Consequently, original gas in place (*OGIP*) can be estimated and well future performance can be forecasted.

DEDICATION

To my parents for their love, sacrifices and prayers.

To my beloved wife, Asmaa, for her love, patience and support throughout my study.

To my adorable son, Hatem, (our little Aggie who was born while I was working on this research and turned one when I defended it), for the joy and happiness he has brought to my life.

ACKNOWLEDGEMENTS

All praises and thanks to Allah almighty, the Lord of the entire creation that exists, for His infinite mercies and abundant blessings.

I would like to thank my committee chair, Dr. Robert Wattenbarger, for his support, guidance and inspiration throughout this research. I was honored to work with him.

I would also like to thank Dr. Maggard and Dr. Rundell for serving on my advisory committee and for their constructive feedback which helps making this work better.

In addition, I would like to express my gratitude to Saudi Aramco for giving me the chance to pursue my advanced degree and sponsoring my study at Texas A&M University.

Thanks to my colleagues at the Reservoir Modeling Consortium for their informative discussions and friendship; namely, Hassan Hamam, Salman Mengal, Tan Tran, Pahala Sinurat, Anas Almarzooq, Haider Abdulaal, Orkhan Samandarli and Ammar Agnia.

Thanks also go to my friends, colleagues and the Petroleum Engineering department faculty and staff for making my time at Texas A&M University a great experience.

Finally, thanks to Saudi Students Association for their support and making College Station our second home.

TABLE OF CONTENTS

CHAPTER Page

CHAPTER Page

LIST OF FIGURES

FIGURE Page

FIGURE Page

LIST OF TABLES

CHAPTER I

INTRODUCTION

A naturally fractured reservoir can be defined as a reservoir that contains a connected network of fractures created by natural processes that have or predicted to have an effect on the fluid flow (Nelson 2001). Naturally fractured reservoirs (NFRs) contain more than 20% of the World's hydrocarbon reserves (Sarma and Aziz 2006). Moreover, most of the unconventional resources such as shale gas are also contained in fractured reservoirs. Horizontal wells are becoming the norm for field development nowadays. In addition, nearly all horizontal wells completed in shale and tight gas reservoirs are hydraulically fractured.

Traditionally, dual-porosity models have been used to model NFRs where all fractures are assumed to have identical properties. Many dual-porosity models have been developed starting by Warren & Root (1963) sugar cube model in which matrix provides the storage while fractures provide the flow medium. The model assumed pseudosteady state fluid transfer between matrix and fractures. Since then several models were developed mainly as variation of the Warren & Root model assuming different matrix-fracture fluid transfer conditions.

This thesis follows the style of *SPE Reservoir Evaluation & Engineering*.

However, it is more realistic to assume fractures having different properties. This is more apparent in case of hydraulically fractured wells. Thus, triple-porosity models have been developed as more realistic models to capture reservoir heterogeneity in NFRs. Models for more than three interacting media are also available in the literature. However, no triple-porosity model has been developed for linear flow in fractured reservoirs. In addition, no triple-porosity (dual fracture) model is available for either linear or radial flow that considers transient fluid transfer between matrix and micro-fractures.

1.1 Motivation

The motivation behind this research was triggered by the Barnett Shale where hydraulically fractured horizontal wells are drilled parallel to the pre-existing natural fractures. It has been documented that hydraulic fractures growth could re-open the pre-existing natural fractures (Gale *et al.* 2007). Therefore, for any model to be used to analyze such wells, it has to account for both natural and hydraulic fractures to be practical.

1.2 Objectives

The objective of this research is to develop analytical solutions to model the fluid flow toward a horizontal well in a triple-porosity reservoir consisting of matrix and two sets of orthogonal fractures that have different properties. These fractures are the more permeable macro-fractures and the less permeable micro-fractures. El-Banbi (1998) linear flow solutions will be used and new fracture functions will be derived.

1.3 Organization of the Thesis

This thesis is divided into seven chapters. The organization of these chapters is as follows:

Chapter I is an introduction to the subject of this research, its motivations and objectives.

Chapter II is devoted for literature review about modeling of fractured reservoirs using dual, triple and multiple-porosity models with emphasis on linear flow.

Chapter III presents the new analytical triple-porosity solutions developed for linear flow towards a horizontal well in triple-porosity reservoirs. The solutions are verified for their mathematical consistency by comparing them with their dual-porosity counterparts. In addition, the applicability of these solutions to radial systems and gas flow are presented.

Chapter IV confirms the analytical solutions by numerical simulation model built using CMG reservoir simulator.

Chapter V presents the non-linear regression as a tool to match field data using the triple-porosity model. Two regression methods are presented: the least squares and the least absolute value.

Chapter VI presents the application of the new model to shale gas horizontal wells. The model uses non-linear regression to match the field data and estimate reservoir parameters.

Chapter VII presents conclusions and recommendations.

CHAPTER II

LITERATURE REVIEW

This chapter provides a literature review of the NFRs modeling. Some of the available dual, triple and multiple-porosity models will be reviewed. In addition, linear flow solutions for fractured reservoirs will be discussed

2.1 Dual-porosity Models

Naturally fractured reservoirs are usually characterized using dual-porosity models. The foundations of dual-porosity models were first introduced by Barenblatt *et al*. (1960). The model assumes pseudosteady state fluid transfer between matrix and fractures. Later, Warren and Root (1963) extended Barenblatt *et al*. model to well test analysis and introduced it to the petroleum literature. The Warren & Root model was mainly developed for transient well test analysis in which they introduced two dimensionless parameters, ω and λ. ω describes the storativity of the fractures system and λ is the parameter governing fracture-matrix flow.

Dual-porosity models can be categorized into two major categories based on the interporosity fluid transfer assumption: pseudosteady state models and unsteady state models.

2.1.1 Pseudosteady State Models

Warren & Root (1963) based their analysis on sugar cube idealization of the fractured reservoir (**Fig. 2.1**). They assumed pseudo-steady state flow between the

matrix and fracture systems. That is, the pressure at the middle of the matrix block starts changing at time zero. In their model, two differential forms (one for matrix and one for fracture) of diffusivity equations were solved simultaneously at a mathematical point. The fracture-matrix interaction is related by

$$q = \alpha \frac{k_m}{\mu}\left(p_m - p_f\right) \quad \text{.....(2.1)}$$

where q is the transfer rate, α is the shape factor, k_m is the matrix permeability, μ is the fluid viscosity and $(p_m - p_f)$ is the pressure difference between the matrix and the fracture.

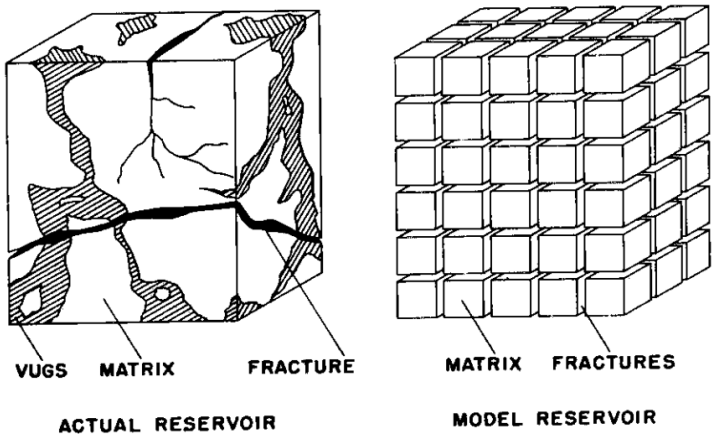

Fig. 2.1 – Idealization of the heterogeneous porous medium (Warren & Root 1963).

2.1.2 Unsteady State Models

Other models (Kazemi 1969; de Swaan 1976; Ozkan *et al.* 1987) assume unsteady-state (transient) flow condition between matrix and fracture systems. Kazemi (1969) proposed the slab dual-porosity model (**Fig. 2.2**) and provided a numerical

solution for dual-porosity reservoirs assuming transient flow between matrix and fractures. His solution, however, was similar to that of Warren & Root except for the transition period between the matrix and fractures systems.

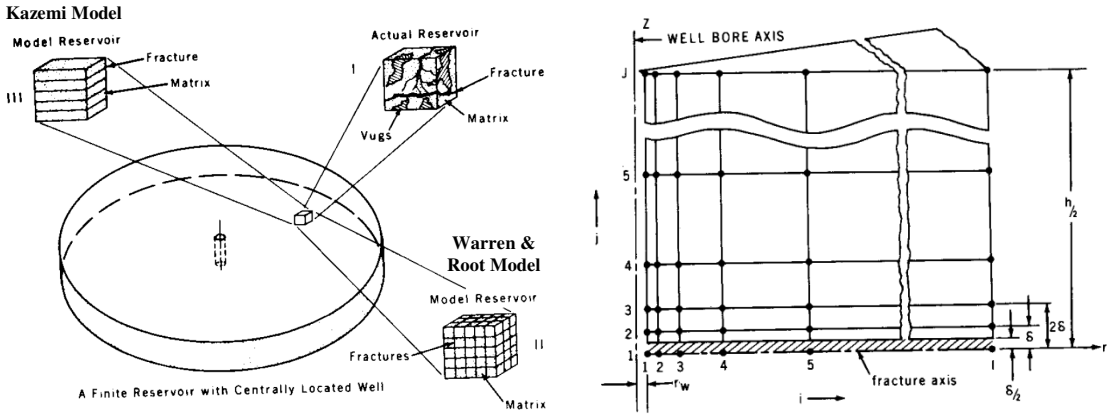

Fig. 2.2 – Idealization of the heterogeneous porous medium (Kazemi 1969).

2.2 Triple-porosity Models

The dual-porosity models assume uniform matrix and fractures properties throughout the reservoir which may not be true in actual reservoirs. An improvement to this drawback is to consider two matrix systems with different properties. This system is a triple-porosity system. Another form of triple-porosity is to consider two fractures systems with different properties in addition to the matrix. The latter is sometimes referred to as dual fracture model.

The first triple-porosity model was developed by Liu (1981, 1983). Liu developed his model for radial flow of slightly compressible fluids through a triple-porosity reservoir under pseudosteady state interporosity flow. The idealization

considers two matrix systems flowing to a single fracture. Asymptotic cases were considered where triple-porosity medium reduces to a single or dual porosity media. This model, however, is rarely referenced as it was not published in the petroleum literature.

In petroleum literature, however, the first triple-porosity model was introduced by Abdassah and Ershaghi (1986). Two geometrical configurations were considered: strata model and uniformly distributed blocks model. In both models, two matrix systems have different properties flowing to a single fracture under gradient (unsteady state) interporosity flow. The solutions were developed for radial system.

Jalali and Ershaghi (1987) investigated the transition zone behavior of the radial triple porosity system. They extended the Abdassah and Ershaghi strata (layered) model by allowing the matrix systems to have different properties and thickness. In addition, three interporosity flow conditions were considered:

a. both matrix systems obey pseudosteady state flow
b. both matrix systems obey unsteady state flow
c. one matrix obeys pseudosteady state while the other obeys unsteady state flow.

Al-Ghamdi and Ershaghi (1996) was the first to introduce the dual fracture triple-porosity model for radial system. Their model consists of a matrix and two fracture systems; more permeable macro-fracture and less permeable micro-fracture. Two sub models were presented. The first is similar to the triple-porosity layered model where micro-fractures replace one of the matrix systems. The second is where the matrix feeds

the micro-fractures under pseudosteady state flow which in turns feed the macro-fractures under pseudosteady state flow condition as well. The macro-fractures and/or micro-fractures are allowed to flow to the well.

Liu *et al*. (2003) presented a radial triple-continuum model. The system consists of fractures, matrix and cavity media. Only the fractures feed the well but they receive flow from both matrix and cavity systems under pseudosteady state condition. Unlike previous triple-porosity models, the matrix and cavity systems are exchanging flow (under pseudosteady state condition) and thus it is called triple-continuum. Their solution was an extension of Warren and Root solution.

Wu *et al*. (2004) used the triple-continuum model for modeling flow and transport of tracers and nuclear waste in the unsaturated zone of Yucca Mountain. The system consists of large fractures, small fractures and matrix. They confirmed the validity of the analytical solution with numerical simulation for injection well injecting at constant rate in a radial system. In addition, they demonstrated the usefulness of the triple-continuum model for estimating reservoir parameters.

Dreier (2004) improved the triple-porosity dual fracture model originally developed by Al-Ghamdi and Ershaghi (1996) by considering transient flow condition between micro-fractures and macro-fractures. Flow between matrix and micro-fractures is still under pseudosteady state condition. His main work (Dreier *et al*. 2004) was the development of new quadruple-porosity sequential feed and simultaneous feed models. He addressed the need for nonlinear regression to match well test data and estimate reservoir properties in case of quadruple porosity model. For the triple-porosity dual

fracture model, the solution was derived in Laplace domain for radial system for a constant rate case with the following fracture function:

$$f(s)=1+\frac{1}{s}\cdot\frac{1}{\kappa}\cdot\frac{1}{h_{D,m}}\cdot\frac{1}{h_{D,fr2}}\cdot\sqrt{f_{fr3}(s)}\cdot\tanh\left(\sqrt{f_{fr3}(s)}\right)$$
$$f_{fr3}(s)=\kappa\cdot h_{D,m}^2\cdot s\cdot\left(\omega_{fr3}+\omega_m\cdot\frac{\lambda}{\omega_m\cdot s+\lambda}\right) \quad \text{.....(2.2)}$$

The dimensionless variables definitions they used are different from these used in this work.

2.3 Linear Flow in Fractured Reservoirs

Linear flow occurs at early time (transient flow) when flow is perpendicular to any flow surface. Wattenbarger (2007) identified different causes for linear transient flow including hydraulic fracture draining a square geometry, high permeability layers draining adjacent tight layers and early-time constant pressure drainage from different geometries.

El-Banbi (1998) developed new linear dual-porosity solutions for fluid flow in linear fractured reservoirs. Solutions were derived in Laplace domain for several inner and outer boundary conditions. These include constant rate and constant pressure inner boundaries and infinite and closed outer boundaries. Skin and wellbore storage effects have been incorporated as well. One important finding is that reservoir functions, $f(s)$, derived for radial flow can be used in linear flow solutions in Laplace domain and vice versa.

Bello (2009) demonstrated that El-Banbi solutions could be used to model horizontal well performance in tight fractured reservoirs. He then applied the constant pressure solution to analyze rate transient in horizontal multi-stage fractured shale gas wells.

Bello (2009) and Bello and Wattenbarger (2008, 2009, 2010) used the dual-porosity linear flow model to analyze shale gas wells. Five flow regions were defined based on the linear dual-porosity constant pressure solution. It was found that shale gas wells performance could be analyzed effectively by region 4 (transient linear flow from a homogeneous matrix). Skin effect was proposed to affect the early flow periods and a modified algebraic equation was proposed to account for it.

Ozkan *et al*. (2009) and Brown *et al.* (2009) proposed a tri-linear model for analyzing well test in tight gas wells. Three contiguous media were considered: finite conductivity hydraulic fractures, dual-porosity inner reservoir between the hydraulic fractures and outer reservoir beyond the tip of the hydraulic fractures. Based on their analysis, the outer reservoir does not contribute significantly to the flow.

Al-Ahmadi *et al*. (2010) presented procedures to analyze shale gas wells using the slab and cube dual-porosity idealizations demonstrated by field examples.

CHAPTER III

TRIPLE-POROSITY MODEL FOR FRACTURED RESERVOIRS: NEW SOLUTIONS

3.1 Introduction

In this chapter, a triple-porosity model is developed and new solutions are derived for linear flow in fractured reservoirs. The triple-porosity system consists of three contiguous porous media: the matrix, less permeable micro-fractures and more permeable macro-fractures. The main flow is through the macro-fractures which feed the well while they receive flow from the micro-fractures only. Consequently, the matrix feeds the micro-fractures only. Therefore, the flow is sequential from one medium to the other. In the petroleum literature, this type of model is sometimes called dual-fracture model.

The problem at hand is to model the fluid flow toward a horizontal well in a triple-porosity reservoir. El-Banbi (1998) solutions for linear flow in dual-porosity reservoirs will be used. However, new reservoir functions will be derived that pertain to the triple-porosity system and can be used in El-Banbi's solutions.

Throughout this thesis, matrix, micro-fractures and macro-fractures are identified with subscripts m, f and F, respectively.

3.2 Linear Flow Solutions for Fractured Linear Reservoirs

El-Banbi (1998) was the first to present solutions to the fluid flow in fractured linear reservoirs. The analytical solutions for constant rate and constant pressure cases in Laplace domain are given by

Constant rate case:
$$\overline{p_{wDL}} = \frac{2\pi}{s\sqrt{s\,f(s)}}\left[\frac{1+\exp\left(-2\sqrt{s\,f(s)}\,y_{De}\right)}{1-\exp\left(-2\sqrt{s\,f(s)}\,y_{De}\right)}\right] \quad \text{.....(3.1)}$$

Constant pressure case:
$$\frac{1}{\overline{q_{DL}}} = \frac{2\pi\, s}{\sqrt{s\,f(s)}}\left[\frac{1+\exp\left(-2\sqrt{s\,f(s)}\,y_{De}\right)}{1-\exp\left(-2\sqrt{s\,f(s)}\,y_{De}\right)}\right] \quad \text{.....(3.2)}$$

Detailed derivations in addition to other solutions are presented in Appendix A.

These solutions can be used to model horizontal wells in dual-porosity reservoirs (Bello 2009). Accordingly, they are equally applicable to triple-porosity reservoirs considered in this work since linear flow is the main flow regime. The fracture function, $f(s)$ however, is different depending on the type of reservoir and imposed assumptions.

3.3 Derivations of the Triple-porosity Analytical Solutions

A sketch of the triple-porosity dual-fracture model is shown in **Fig. 3.1**. The arrows shows the flow directions where fluids flow from matrix to micro-fractures to the macro-fractures and finally to the well.

3.3.1 Model Assumptions

The analytical solutions are derived under the following assumptions:

1. Fully penetrating horizontal well at the center of a closed rectangular reservoir producing at a constant rate
2. Triple-porosity system made up of matrix, less permeable micro-fractures and more permeable macro-fractures
3. Each medium is assumed to be homogenous and isotropic
4. Matrix blocks are idealized as slabs
5. Flow is sequential from one medium to the other; form matrix to micro-fractures to macro-fractures
6. Flow of slightly compressible fluid with constant viscosity

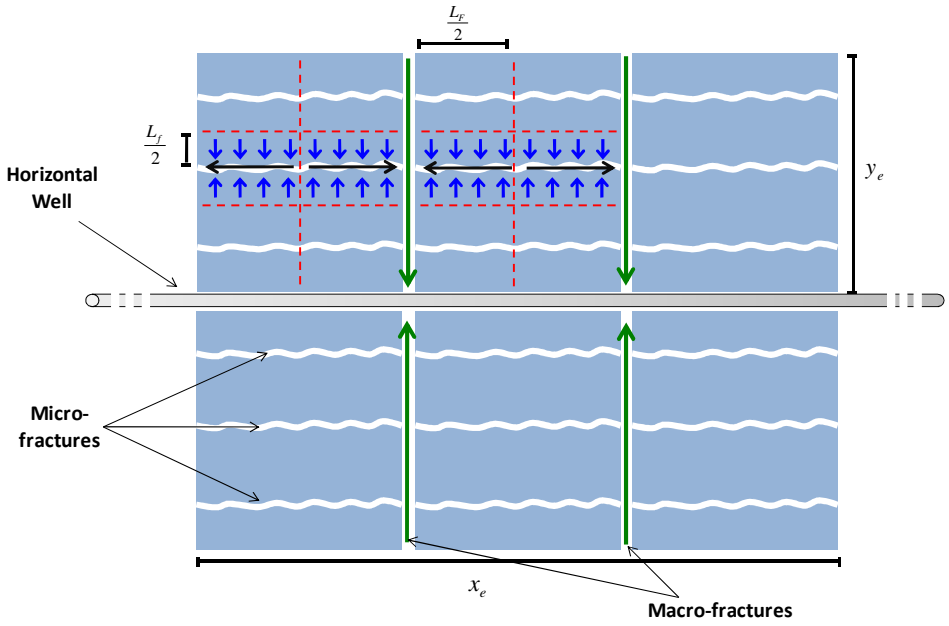

Fig. 3.1 – Top view of a horizontal well in a triple-porosity system with sequential flow. Arrows indicate flow directions.

Four sub-models of the triple-porosity model are derived. The main difference is the assumption of interporosity flow condition, i.e., pseudosteady state or transient. These models are shown graphically in **Fig. 3.2**. The analytical solution for each model is derived in the following sections.

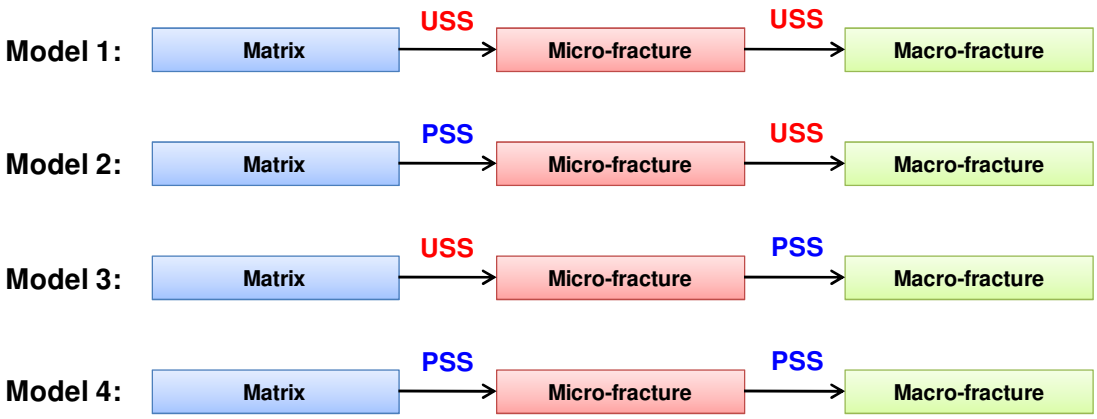

Fig. 3.2 – Sub-models of the triple-porosity model based on different interporosity flow condition assumptions. PSS: pseudosteady state. USS: unsteady state or transient. Arrows indicate flow directions.

3.3.2 Definitions of Dimensionless Variables

Before proceeding with the derivations, the dimensionless variables are defined.

$$t_{DAc} = \frac{0.00633 k_F t}{[\varphi c_t]_t \mu A_{cw}} \quad \text{.....(3.3)}$$

$$p_{DL} = \frac{k_F \sqrt{A_{cw}} (p_i - p)}{141.2 qB\mu} \quad \text{.....(3.4)}$$

$$\omega_F = \frac{[\varphi V c_t]_F}{[\varphi V c_t]_t} \quad \text{.....(3.5)}$$

$$\omega_f = \frac{[\varphi V c_t]_f}{[\varphi V c_t]_t} \quad \text{.....(3.6)}$$

$$\omega_m = \frac{[\varphi V c_t]_m}{[\varphi V c_t]_t} = 1 - \omega_F - \omega_f \quad \text{.....(3.7)}$$

$$\lambda_{Ac,Ff} = \frac{12}{L_F^2}\frac{k_f}{k_F} A_{cw} \quad \text{.....(3.8)}$$

$$\lambda_{Ac,fm} = \frac{12}{L_f^2}\frac{k_m}{k_F} A_{cw} \quad \text{.....(3.9)}$$

$$z_D = \frac{z}{L_f/2} \quad \text{.....(3.10)}$$

$$x_D = \frac{x}{L_F/2} \quad \text{.....(3.11)}$$

$$y_D = \frac{y}{\sqrt{A_{cw}}} \quad \text{.....(3.12)}$$

ω and λ are the storativity ratio and interporosity flow parameter, respectively. k_F and k_f are the bulk (macroscopic) fractures permeabilities

3.3.3 Model 1: Fully Transient Triple-porosity Model

The first sub-model, Model 1, is the fully transient model. The flow between matrix and micro-fractures and that between micro-fractures and macro-fractures are under transient condition. This model is an extension to the dual-porosity transient slab model (Kazemi 1969 Model). The derivation starts by writing the differential equations describing the flow in each medium.

The matrix equation:

$$\frac{\partial^2 p_m}{\partial z^2} = \left(\frac{\varphi \mu c_t}{k}\right)_m \frac{\partial p_m}{\partial t} \quad \text{.....(3.13)}$$

The initial and boundary conditions are

Initial condition: $p_m(z,0) = p_i$

Inner boundary: $\frac{\partial p_m}{\partial z} = 0 \qquad @ \quad z = 0$

Outer boundary: $p_m = p_f \qquad @ \quad z = \frac{L_f}{2}$

The micro-fractures equation:

$$\frac{\partial^2 p_f}{\partial x^2} = \left(\frac{\varphi \mu c_t}{k}\right)_f \frac{\partial p_f}{\partial t} + \frac{1}{L_f/2} \frac{k_m}{k_f} \frac{\partial p_m}{\partial z}\bigg|_{z=L_f/2} \quad \text{.....(3.14)}$$

The initial and boundary conditions are

Initial condition: $p_f(x,0) = p_i$

Inner boundary: $\frac{\partial p_f}{\partial x} = 0 \qquad @ \quad x = 0$

Outer boundary: $p_f = p_F \qquad @ \quad x = \frac{L_F}{2}$

And the macro-fractures equation:

$$\frac{\partial^2 p_F}{\partial y^2} = \left(\frac{\varphi \mu c_t}{k}\right)_F \frac{\partial p_F}{\partial t} + \frac{1}{L_F/2} \frac{k_f}{k_F} \frac{\partial p_f}{\partial x}\bigg|_{x=L_F/2} \quad \text{.....(3.15)}$$

The initial and boundary conditions are

Initial condition: $p_F(y,0) = p_i$

Inner boundary: $q = -\frac{k_F A_{cw}}{\mu} \frac{\partial p_F}{\partial y}\bigg|_{y=0}$

Outer boundary: $\frac{\partial p_F}{\partial y} = 0 \qquad @ \quad y = y_e$

Using dimensionless variables definitions in Eq. 3.3 to 3.12, Eq. 3.13 to 3.15 can be rewritten as

Matrix: $$\frac{\partial^2 p_{DLm}}{\partial z_D^2} = \left(1-\omega_f-\omega_F\right)\frac{3}{\lambda_{Ac,fm}}\frac{\partial p_{DLm}}{\partial t_{DAc}} \quad \text{.....(3.16)}$$

Micro-fractures: $$\frac{\partial^2 p_{DLf}}{\partial x_D^2} = \omega_f \frac{3}{\lambda_{Ac,Ff}}\frac{\partial p_{DLf}}{\partial t_{DAc}} + \frac{\lambda_{Ac,fm}}{\lambda_{Ac,Ff}}\frac{\partial p_{DLm}}{\partial z_D}\bigg|_{z_D=1} \quad \text{.....(3.17)}$$

Macro-fractures: $$\frac{\partial^2 p_{DLF}}{\partial y_D^2} = \omega_F \frac{\partial p_{DLF}}{\partial t_{DAc}} + \frac{\lambda_{Ac,Ff}}{3}\frac{\partial p_{DLf}}{\partial x_D}\bigg|_{x_D=1} \quad \text{.....(3.18)}$$

The initial and boundary conditions in dimensionless form are as follows:

Matrix:

Initial condition: $p_{DLm}(z_D,0)=0$

Inner boundary: $\frac{\partial p_{DLm}}{\partial z_D}=0 \quad @ \ z_D=0$

Outer boundary: $p_{DLm}=p_{DLf} \quad @ \ z_D=1$

Micro-fractures:

Initial condition: $p_{DLf}(x_D,0)=0$

Inner boundary: $\frac{\partial p_{DLf}}{\partial x_D}=0 \quad @ \ x_D=0$

Outer boundary: $p_{DLf}=p_{DLF} \quad @ \ x_D=1$

Macro-fractures:

Initial condition: $p_{DLF}(y_D,0)=0$

Inner boundary: $\frac{\partial p_{DLF}}{\partial y_D}\bigg|_{y_D=0}=-2\pi$

Outer boundary: $\frac{\partial p_{DLF}}{\partial y_D}=0 \quad @ \ y_D=y_{De}={}^{y_e}\!\!\diagup\!\!_{\sqrt{A_{cw}}}$

The system of differential equations, Eqs. 3.16 to 3.18, can be solved using Laplace transformation as detailed in Appendix B. The fracture function, $f(s)$, for this model is given by

$$f(s) = \omega_F + \frac{\lambda_{Ac,Ff}}{3s}\sqrt{s\,f_f(s)}\,\tanh\left(\sqrt{s\,f_f(s)}\right)$$
$$f_f(s) = \frac{3\omega_f}{\lambda_{Ac,Ff}} + \frac{\lambda_{Ac,fm}}{s\,\lambda_{Ac,Ff}}\sqrt{\frac{3s\,\omega_m}{\lambda_{Ac,fm}}}\,\tanh\left(\sqrt{\frac{3s\,\omega_m}{\lambda_{Ac,fm}}}\right) \quad \text{.....(3.19)}$$

Using the fracture function, Eq. 3.19 in Eqs. 3.1 or 3.2 will give the triple-porosity fully transient model response for constant rate or constant pressure cases, respectively in Laplace domain. The solution can then be inverted to real (time) domain using inverting algorithms like Stehfest Algorithm (Stehfest 1970).

3.3.4 Model 2: Mixed Flow Triple-porosity Model

The second sub-model, Model 2, is where the interporosity flow between matrix and micro-fractures is under pseudosteady state while it is transient between micro-fractures and macro-fractures.

Following the same steps for Model 1, the fracture function for this model is given by (details are shown in Appendix C)

$$f(s) = \omega_F + \frac{\lambda_{Ac,Ff}}{3s}\sqrt{s\,f_f(s)}\,\tanh\left(\sqrt{s\,f_f(s)}\right)$$
$$f_f(s) = \frac{3\omega_f}{\lambda_{Ac,Ff}} + \frac{3\omega_m\lambda_{Ac,fm}}{s\omega_m\lambda_{Ac,Ff} + \lambda_{Ac,fm}\lambda_{Ac,Ff}} \quad \text{.....(3.20)}$$

A similar model was derived by Dreier *et al* (2004) for radial flow. However, their fracture function is different since they had different definitions of dimensionless variables and used intrinsic properties for the transient flow.

3.3.5 Model 3: Mixed Flow Triple-porosity Model

The third sub-model, Model 3, is where the flow between the matrix and micro-fractures is transient while the flow between micro-fractures and macro-fractures is pseudosteady state. It is the opposite of Model 2.

The derived fracture function for this model as detailed in Appendix D is given by

$$f(s)=\omega_F+\frac{3\omega_f\lambda_{Ac,Ff}+\dfrac{\lambda_{Ac,Ff}\lambda_{Ac,fm}}{s}\sqrt{\dfrac{3s\omega_m}{\lambda_{Ac,fm}}}\tanh\left(\sqrt{\dfrac{3s\omega_m}{\lambda_{Ac,fm}}}\right)}{3\lambda_{Ac,Ff}+3s\omega_f+\lambda_{Ac,fm}\sqrt{\dfrac{3s\omega_m}{\lambda_{Ac,fm}}}\tanh\left(\sqrt{\dfrac{3s\omega_m}{\lambda_{Ac,fm}}}\right)} \quad \text{.....(3.21)}$$

3.3.6 Model 4: Fully PSS Triple-porosity Model

The fourth sub-model, Model 4, is the fully pseudosteady state model. The flow between all three media is under pseudosteady state. This model is an extension of the Warren & Root dual-porosity pseudosteady state model. The derived fracture function as detailed in Appendix E is given by

$$f(s)=\omega_F+\frac{\lambda_{Ac,Ff}\left[\omega_m\lambda_{Ac,fm}+\omega_f\left(s\omega_m+\lambda_{Ac,fm}\right)\right]}{\left(\lambda_{Ac,Ff}+s\omega_f\right)\left(s\omega_m+\lambda_{Ac,fm}\right)+s\omega_m\lambda_{Ac,fm}} \quad \text{.....(3.22)}$$

This model is also a limiting case of Liu *et al* (2000; Wu *et al*, 2004) triple-continuum model if considering sequential flow and ignoring the flow component between matrix and macro-fractures.

3.3.7 Triple-porosity Solutions Comparison

Models 1 through 4 cover all possibilities of fluid flow in triple-porosity system under sequential flow assumption. Comparison of the constant pressure solution based on these models is shown in **Fig. 3.3**. As can be seen on the figure, Models 1 and 4 represents the end members while Models 2 and 3 are combination of these models. Model 2 follows Model 1 at early time but follows Model 4 at later time while Model 3 is the opposite.

Considering rate transient analysis, Models 1 and 3 are more likely to be applicable to field data.

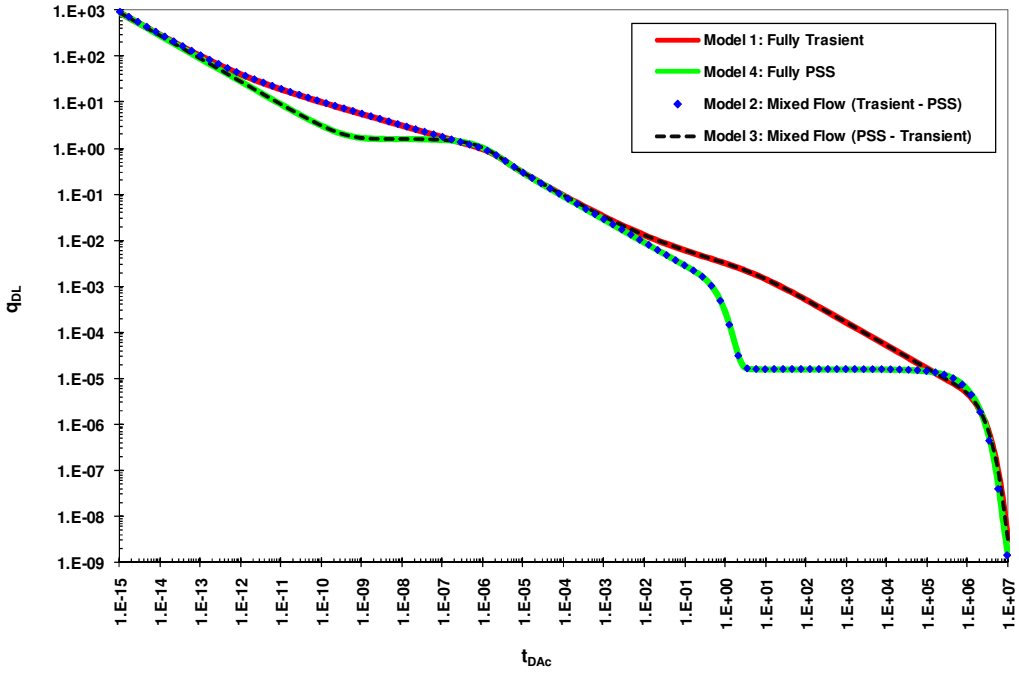

Fig. 3.3 – Comparison of the constant pressure solutions based on the four triple-porosity models.

3.4 Mathematical Consistency of the Analytical Solutions

In this section, the solutions mathematical consistency is checked by reducing the triple-porosity model to its dual-porosity counterpart. This can be achieved by allowing the micro-fractures to dominate the flow and assigning to them the dual-porosity matrix properties from the dual-porosity system. In this case, the matrix-micro-fractures interporosity coefficient, $\lambda_{Ac,fm}$, is very small and the triple-porosity matrix storativity ratio, ω, is zero. This comparison is shown for all models in the following figures. **Table 3.1** shows the data used for comparison.

Table 3.1 – Input parameters for dual and triple-porosity solutions comparison			
Dual-Porosity Parameters		Triple-Porosity Parameters	
ω	0.001	ω_F	0.001
λ	0.005	ω_f	0.999
y_{eD}	10	$\lambda_{Ac,Ff}$	0.005
		$\lambda_{Ac,fm}$	1×10^{-9}
		y_{eD}	10

Models 1 and 2 are reduced to the transient slab dual-porosity model since the flow between micro-fractures and macro-fractures is under transient conditions in the two models. As shown **Fig. 3.4**, the triple-porosity solutions are identical to their dual-porosity counterpart. This confirms the mathematical consistency of Models 1 and 2.

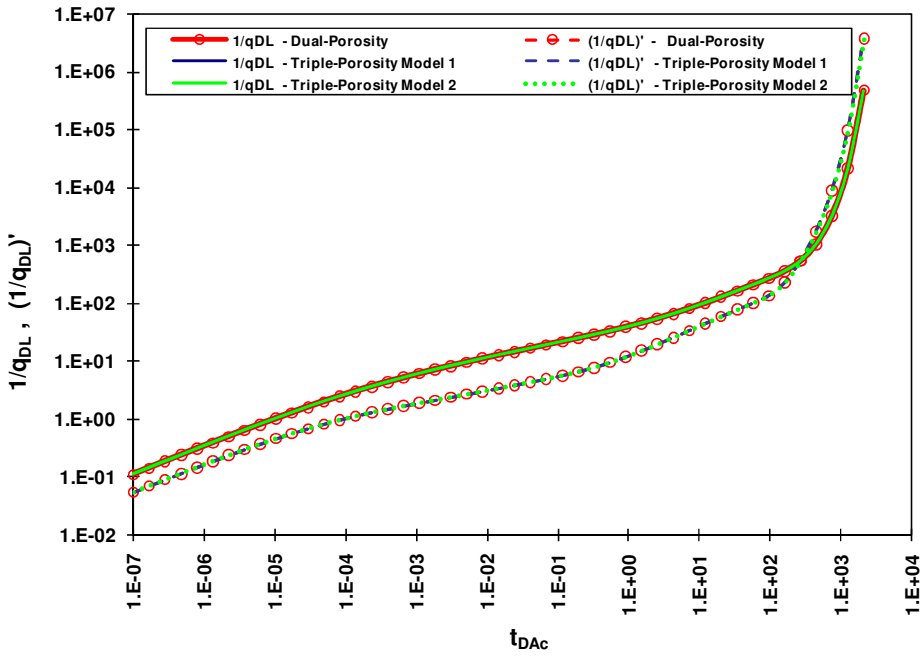

Fig. 3.4 –A log-log plot of transient dual-porosity (DP) and triple-porosity (TP) Models 1 and 2 solutions for constant pressure case. The two solutions are identical indicating the mathematical consistency of the new triple-porosity solutions.

Models 3 and 4, however, are reduced to the pseudosteady state dual-porosity model since the flow between micro-fractures and macro-fractures is under pseudosteady state condition in the two models. As shown in **Fig. 3.5**, the triple-porosity solutions are identical to their dual-porosity counterpart. This confirms the mathematical consistency of Models 3 and 4.

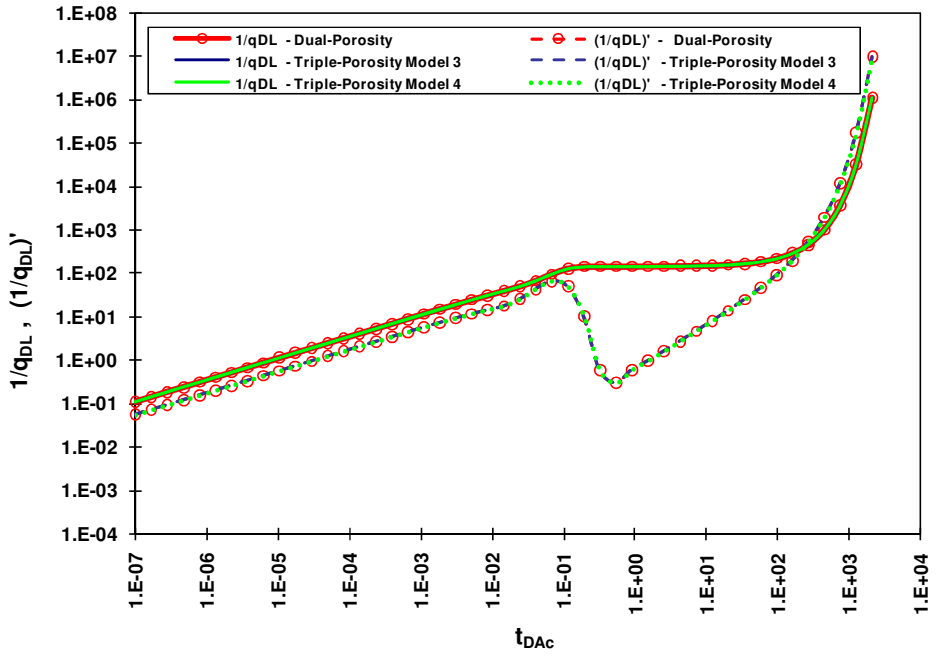

Fig. 3.5 – A log-log plot of pseudosteady state dual-porosity (DP) and triple-porosity (TP) Models 3 and 4 solutions for constant pressure case. The two solutions are matching indicating the mathematical consistency of the new triple-porosity solutions.

3.5 Flow Regions Based on the Analytical Solution

Since Model 1, the fully transient model, is the most general of all the four triple-porosity variations and shows all possible flow regions, all discussions in this section and the following chapters will be limited to Model 1. Based on Model 1 constant

pressure solution, six flow regions can be identified as the pressure propagates through the triple-porosity system. These flow regions are shown graphically on the log-log plot of dimensionless rate versus dimensionless time in **Fig 3.6**. Regions 1 through 5 exhibit an alternating slopes of – ½ and – ¼ indicating linear and bilinear transient flow, respectively. Region 6 is the boundary dominated flow and exhibits an exponential decline due to constant bottom-hole pressure. These flow regions are explained in details in the following sections. Appendix F shows the effect of each solution parameter on Model 1 response for constant pressure case.

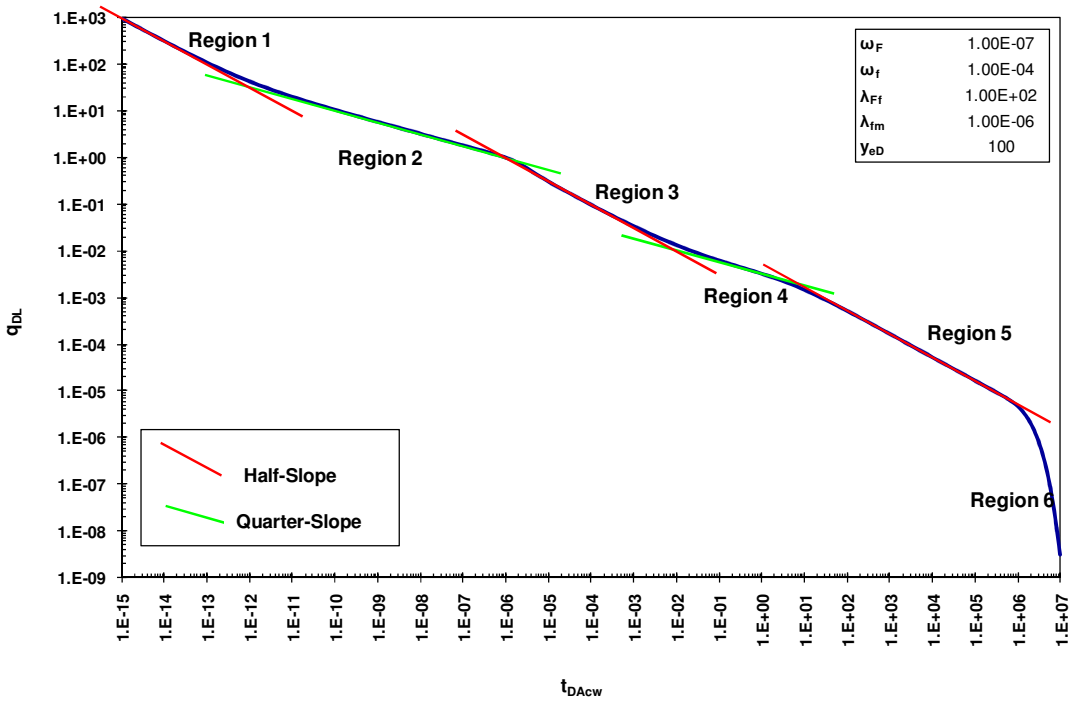

Fig. 3.6 – A log-log plot of triple-porosity solution. Six flow regions can be identified for Model 1 constant pressure solution. Slopes are labeled on the graph.

3.5.1 Region 1

Region 1 represents the transient linear flow in the macro-fractures only. The permeability of macro-fractures is usually high and hence, in most cases, this flow region will be very short. It may not be captured by most well rate measurement tools. This flow region exhibits a half-slope on the log-log plot of rate versus time.

3.5.2 Region 2

Region 2 is the bilinear flow in the macro-fractures and micro-fractures. It is caused by simultaneous perpendicular transient linear flow in the micro-fractures and the macro-fractures. This flow region exhibit a quarter-slope on the log-log plot of rate versus time.

3.5.3 Region 3

Region 3 is the linear flow in the micro-fractures system. It will occur once the transient flow in the macro-fractures ends indicating the end of bilinear flow (region 2). This flow region exhibits a half-slope on the log-log plot of rate versus time.

3.5.4 Region 4

Region 4 is the bilinear flow in the micro-fractures and matrix. It is caused by the linear flow in the matrix while the micro-fractures are still in transient flow. This flow region exhibits a quarter-slope on the log-log plot of rate versus time. In most field cases, this flow region is the first one to be observed.

3.5.5 Region 5

Region 5 is the main and longest flow region in most field cases. It is the linear flow out of the matrix to the surrounding micro-fractures. This region exhibits a half-slope on the log-log plot of rate versus time. Analysis of this region will allow the estimation of fractures surface area available to flow, A_{cm}.

3.5.6 Region 6

Region 6 is the boundary dominated flow. It starts when the pressure at the center of the matrix blocks starts to decline. This flow is governed by exponential decline due to constant bottom-hole pressure.

3.6 Triple-porosity Solutions for Radial Flow

Although the triple-porosity solutions were derived for linear flow, they are equally applicable to radial flow following El-Banbi (1998) work. The differential equation in Laplace domain that governs the flow in the macro-fractures in case of radial system is given by

$$\frac{1}{r_D}\frac{\partial}{\partial r_D}\left(r_D\frac{\partial \overline{p_{DF}}}{\partial r_D}\right)-s\,f(s)\,\overline{p_{DF}}=0 \quad \text{.....(3.23)}$$

The constant pressure solution for a closed reservoir is given by (El-Banbi 1998)

$$\frac{1}{\overline{q_D}}=\frac{s\left[I_0\left(\sqrt{s\,f(s)}\right)K_1\left(\sqrt{s\,f(s)}\,r_{eD}\right)+I_1\left(\sqrt{s\,f(s)}\,r_{eD}\right)K_0\left(\sqrt{s\,f(s)}\right)\right]}{\sqrt{s\,f(s)}\left[I_1\left(\sqrt{s\,f(s)}\,r_{eD}\right)K_1\left(\sqrt{s\,f(s)}\right)+I_1\left(\sqrt{s\,f(s)}\right)K_1\left(\sqrt{s\,f(s)}\,r_{eD}\right)\right]} \quad \text{.....(3.24)}$$

The fractures functions, $f(s)$, derived for all the models can be used in the radial flow solutions as well. **Fig. 3.7** shows comparison between radial dual-porosity solutions

and the new triple-porosity solutions reduced to their dual-porosity counterpart and applied to radial flow. Data used for comparison are shown in **Table 3.2**.

The solutions are identical indicating the applicability of the new triple-porosity solutions derived in this work to radial flow.

Table 3.2 – Input parameters for dual and triple-porosity solutions comparison for radial flow

Dual-Porosity Parameters		Triple-Porosity Parameters	
ω	0.001	ω_F	0.001
λ	0.001	ω_f	0.999
r_{eD}	10	$\lambda_{Ac,Ff}$	0.001
		$\lambda_{Ac,fm}$	1×10^{-9}
		r_{eD}	10

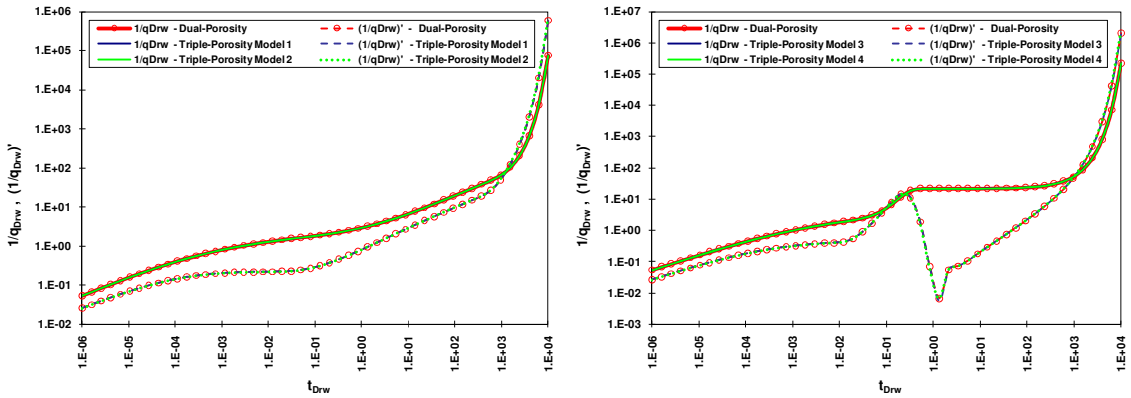

Fig. 3.7 – Log-log plot of dual-porosity and triple-porosity constant pressure solutions for radial flow.

3.7 Application to Gas Flow

It is important to note that the above solutions were derived for slightly compressible fluids and thus are applicable to liquid flow only. However, they can be applied to gas flow by using gas potential, $m(p)$, instead of pressure to linearize the left-hand side of the diffusivity equation. Therefore, the dimensionless pressure variable will be defined in terms of gas potential as

$$m_{DL} = \frac{k_F \sqrt{A_{cw}}\left[m(p_i) - m(p)\right]}{1422\, q_g\, T} \quad \text{.....(3.25)}$$

where $m(p)$ is the gas potential defined as (Al-Hussainy *et al*. 1966)

$$m(p) = 2\int_{p_0}^{p} \frac{p}{z\,\mu} dp \quad \text{.....(3.26)}$$

With the above linearization, the derived solutions are applicable to the transient flow regime for gas flow. However, once the reservoir boundaries are reached and average reservoir pressure starts to decline, the gas properties will change considerably especially the gas viscosity and compressibility. Therefore, the solutions have to be corrected for changing fluid properties. This is usually achieved by using pseudo-time or material balance time. An example of these transformations is the Fraim and Wattenbarger (1987) normalized time defined as

$$t_n = \int_0^t \frac{(\mu c_t)_i}{\mu(\bar{p}) c_t(\bar{p})} d\tau \quad \text{.....(3.27)}$$

Thus, with these two modifications, the analytical solutions derived in this work are applicable to gas flow.

3.8 Chapter Summary

In this chapter, four new triple-solutions have been developed to model the fluid flow in a triple-porosity (dual-fracture) system under sequential flow assumption. Six flow regions were identified based on this model. According to the best knowledge of the author, the triple-porosity model for linear fractured reservoirs is new and has not been presented in the literature before. In addition, even for radial reservoirs these solutions are new and have not been presented before in this form.

CHAPTER IV

TRIPLE-POROSITY SIMULATION MODEL AND ANALYTICAL SOLUTIONS VERIFICATION

4.1 Introduction

In this chapter, a triple-porosity simulation model is built using CMG reservoir simulator. The objective is to understand the behavior of triple-porosity reservoirs and to verify the analytical solutions derived in Chapter III.

The model considers the flow toward a horizontal well in a triple-porosity reservoir. One representative segment is modeled which represents one quadrant of the reservoir volume around a macro-fracture.

4.2 Simulation Model Description

The model was built with the CMG reservoir simulator. Only one segment was simulated representing one quadrant of the reservoir volume around one macro-fracture. This segment contains ten micro-fractures orthogonal to the macro-fractures at 20 ft fracture spacing. The model is a 2-D model with 21 gridcells in the x-direction, 211 gridcells in y-direction and only one cell in the z-direction. A top view of the model is shown in **Fig. 4.1**. All matrix, micro-fractures and macro-fractures properties are assigned explicitly. In addition, the simulation model assumes connate water saturation for both oil and gas cases.

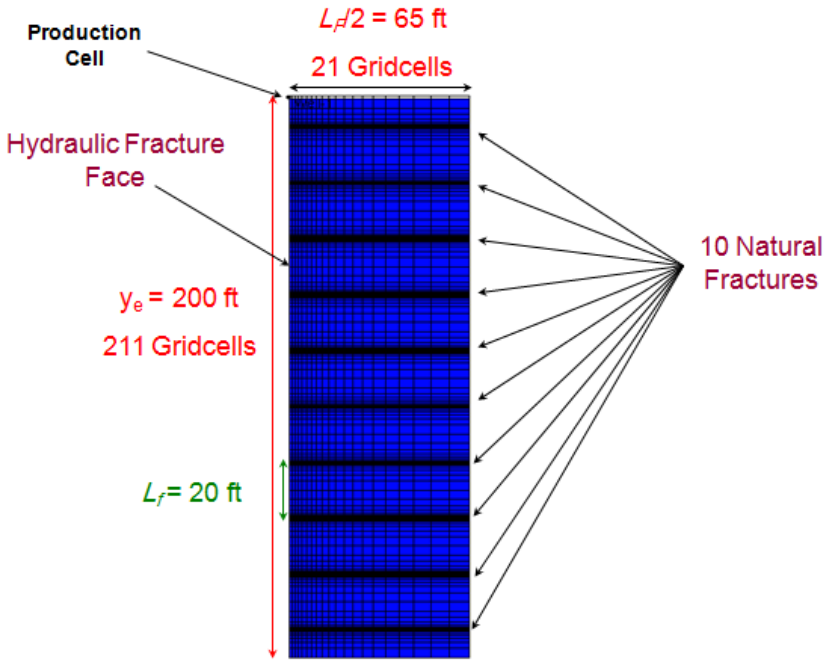

Fig. 4.1 – Top view of the CMG 2-D triple-porosity simulation model.

4.3 Analytical Solution Validation

The simulator was run for many cases by changing the three porosities and permeabilities of the three media. In order to validate the analytical solution derived in Chapter III, the simulation results are compared to that of the analytical solutions for each case. All cases were matched with analytical solutions and thus confirming their validity. Results of two comparison runs are presented here: one for oil and the other for gas as shown in **Figs. 4.2** and **4.3**, respectively.

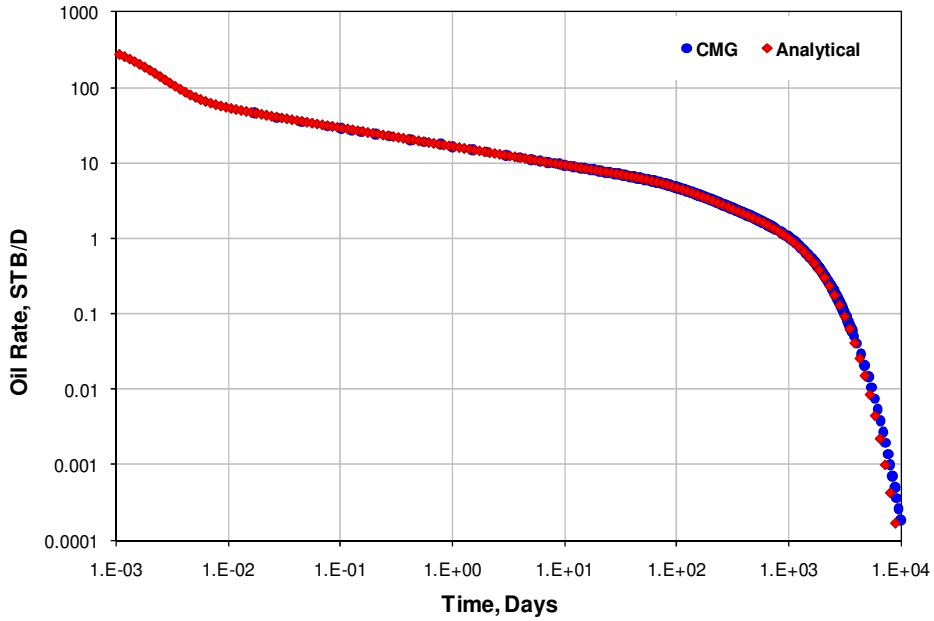

Fig. 4.2 – Match between simulation and analytical solution results for an oil case. ($k_{F,in}$ = 1000 md, $k_{f,in}$ = 1 md and k_m = 1.5×10^{-4} md).

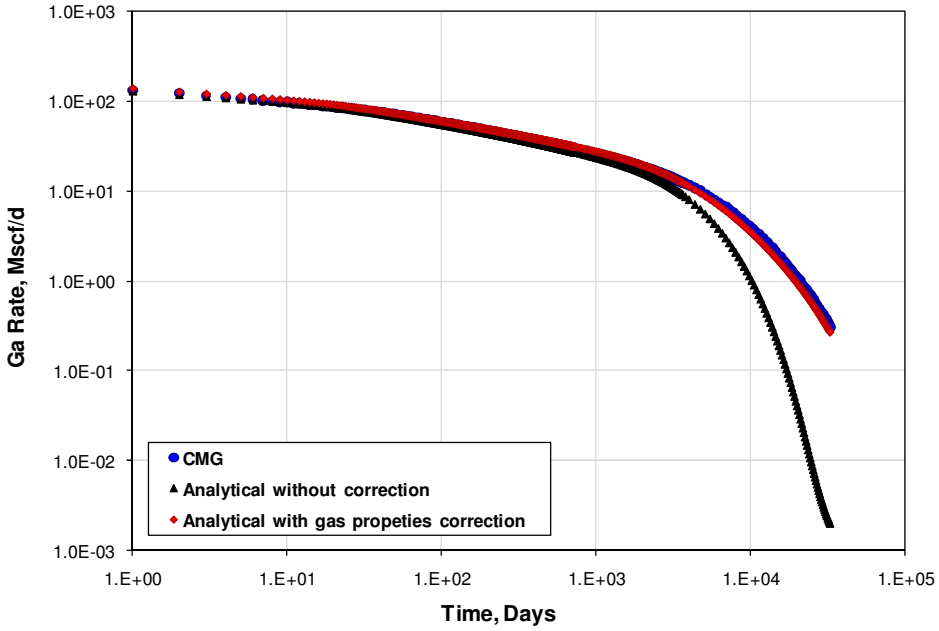

Fig. 4.3 – Simulation and analytical solution match for a gas case. The boundary dominated flow was matched very well after correcting for changing gas properties. ($k_{F,in}$ = 2 md, $k_{f,in}$ = 0.1 md and k_m = 1.5×10^{-4} md).

4.4 Limiting Cases

In order to confirm the integrity of the simulation model and the analytical solution, asymptotic cases were run in which the triple-porosity system will reduce to a simpler system, i.e., dual-porosity or homogenous system.

The first case is to assign a very high permeability to the macro-fractures. Thus, the transient flow in the macro-fracture will be very fast and the system will act as if it is dual-porosity system, i.e., the macro-fractures are effectively eliminated. The results are shown in **Fig. 4.4**. The triple-porosity and dual-porosity solutions are matching the simulation results. This indicates that the system can be effectively described by dual-porosity model. In addition, the triple-porosity is matching the dual-porosity solution indicating that the new solution is valid.

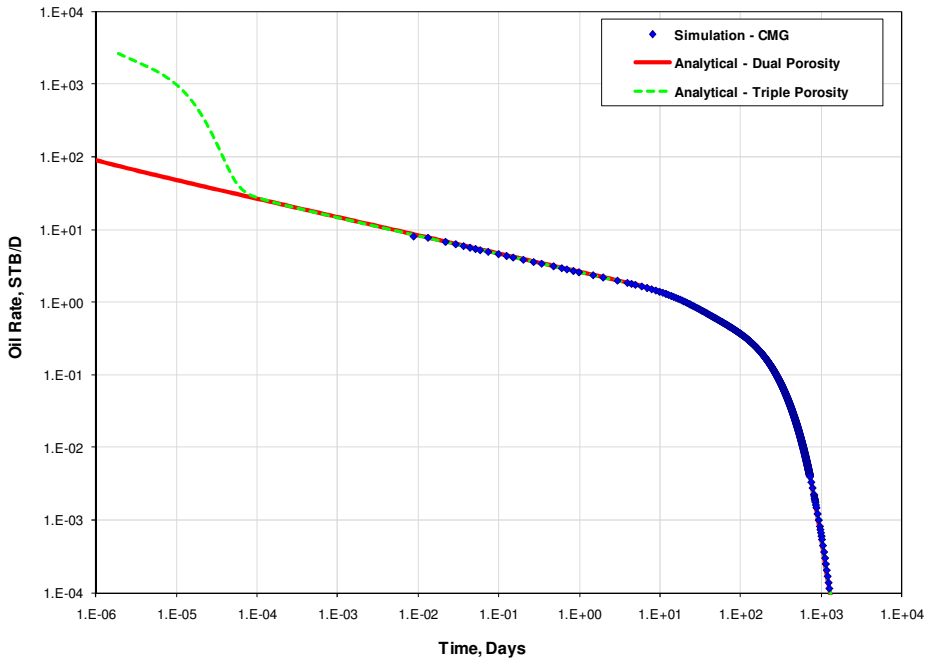

Fig. 4.4 – Simulation and analytical solutions match for the triple-porosity system with high macro-fractures permeability.

In the second limiting case, both macro and micro-fractures permeabilities were assigned very high values. Thus, the transient flow in both fractures system will be very fast and end in less than a day. Hence, the system behaves as if it is homogenous linear flow, i.e., micro and macro-fractures are effectively eliminated. The results of this case are shown in **Fig. 4.5**.

The simulation results were matched perfectly with all solutions. This indicates that the system can be modeled using any of the analytical solutions and more importantly confirms the validity of the triple-porosity solution.

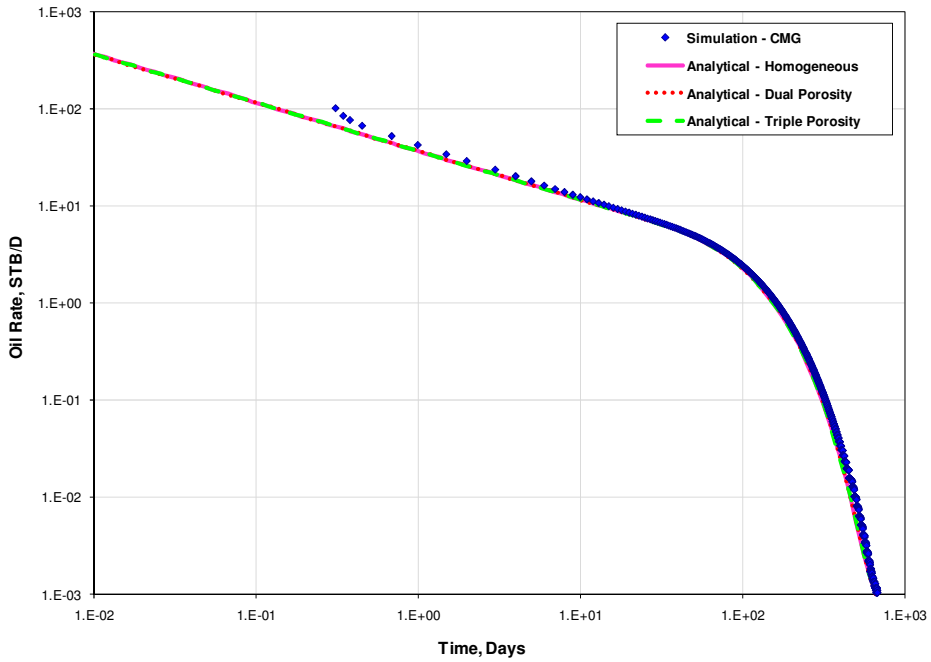

Fig. 4.5 – Simulation and analytical solutions match for the triple-porosity system with high micro-fractures and macro-fractures permeability.

4.5 Chapter Summary

The triple-porosity fully transient (Model 1) solution was confirmed with reservoir simulation for both liquid and gas flow. Correcting the time for gas properties before calculating the model response for gas case helps in applying the model for gas flow as well. Limiting cases prove the validity of both analytical solutions and the simulation model.

CHAPTER V

NON-LINEAR REGRESSION

5.1 Introduction

The model derived in Chapter III needs at most five parameters; namely two ω's, two λ's and y_{De}. In addition, these calculated parameters depend on reservoir properties which have to be estimated. This leads to estimation of many parameters that may not be known or needs to be calculated. Therefore, the need for regression arises in order to match field data and have a good estimate of the sought reservoir or well parameters.

In automated well test interpretations, the common regression methods are the least squares, least absolute value and modified least absolute value minimization. The least squares and the least absolute value methods are described below.

5.2 Least Squares Method

Least squares (LS) regression method is the most popular regression method in well test analysis. It minimizes the sum of squares of residuals between the measured and calculated values, well rates in this case. For the purpose of this research, the available data is series of rate and time, $\{t_i, q_{meas,i}\}$. Defining $\vec{\alpha}$ as the vector containing the reservoir/well parameters to be estimated, the objective function is then defined as

$$E = \sum_{i=1}^{n} \left[q_{meas,i} - q_{calc,i}(\vec{\alpha}, t_i) \right]^2 \quad \text{.....(5.1)}$$

Since the calculated rate function is not a linear function of the parameters in the vector $\vec{\alpha}$, the objective function is approximated by expanding it using Taylor series

expansion up to the second order term around an initial guess of unknown vector, $\vec{\alpha}^0$ as (Rosa & Horne 1995)

$$E^* = E\big|_{\vec{\alpha}^0} + \Delta\vec{\alpha}^T \cdot \vec{g} + \frac{1}{2}\Delta\vec{\alpha}^T \cdot H \cdot \Delta\vec{\alpha} \quad \text{.....(5.2)}$$

where

$$\Delta\vec{\alpha} = \vec{\alpha} - \vec{\alpha}^0 \quad \text{.....(5.3)}$$

$\vec{g}$ is the objective function gradient defined as

$$\vec{g} \equiv \{g_j\} = \left\{\left[\frac{\partial E}{\partial \alpha_j}\right]_{\vec{\alpha}^0}\right\} = -2\sum_{i=1}^{n}\left\{\left[q_{meas,i} - q_{calc,i}\left(\vec{\alpha}^0, t_i\right)\right]\left(\frac{\partial q_{calc,i}\left(\vec{\alpha}^0, t_i\right)}{\partial \alpha_j}\right)_{\vec{\alpha}^0}\right\} \quad \text{.....(5.4)}$$

and H is the Hessian matrix defined as

$$H \equiv \{H_{jk}\} = \left\{\left[\frac{\partial^2 E}{\partial \alpha_k \partial \alpha_j}\right]_{\vec{\alpha}^0}\right\} = -2\sum_{i=1}^{n}\left[-\frac{\partial q_{calc,i}\left(\vec{\alpha}^0, t_i\right)}{\partial \alpha_k} \cdot \frac{\partial q_{calc,i}\left(\vec{\alpha}^0, t_i\right)}{\partial \alpha_j}\right]_{\vec{\alpha}^0} \quad \text{.....(5.5)}$$

The second order derivatives in Eq. 5.5 are neglected to ensure that the objective function will converge to a minimum value. This is known as Newton-Gauss method.

In order to minimize the objective function, its derivative with respect to unknown vector must be zero at the solution point. That is,

$$\frac{\partial E^*}{\partial\left(\Delta\vec{\alpha}\right)} = 0 \quad \text{.....(5.6)}$$

Upon substituting Eq. 5.2 in Eq. 5.6, we have

$$H\,\Delta\vec{\alpha} = -\vec{g} \quad \text{.....(5.7)}$$

The above equation is to be solved iteratively for $\Delta\vec{\alpha}$ since E^* is an approximation of the objective function. Eq. 5.7 can be solved using Gauss Algorithm (Cheney and Kincaid 1985).

The line search algorithm (Rosa and Horne 1995, 1996) is used with upper and lower limits for each parameter. The updated value of solution vector is then calculated as

$$\vec{\alpha}^{k+1} = \vec{\alpha}^k + \rho\Delta\vec{\alpha}^k \quad \text{.....(5.8)}$$

The step length, ρ, is given by

$$\rho = (1/2)^m \quad \text{.....(5.9)}$$

where m is zero at the beginning of each iteration and increases if the new value of $\vec{\alpha}$ is outside the limits or if the value of the objective function fails to decrease until an acceptable solution is obtained. Convergence is achieved when the following criterion is satisfied:

$$\left|\vec{\alpha}^{k+1} - \vec{\alpha}^k\right| \le 10^{-4}\vec{\alpha}^k \quad \text{.....(5.10)}$$

5.3 Least Absolute Value Method

The standard least squares method works better for smooth data. Outliers affect the least squares results since it assigns similar weights for all data points. This can be overcome by introducing a weight factor that becomes very small for outliers. However, a better method is the least absolute value (LAV) method (Rosa and Horne 1995).

While the least-squares method minimizes the sum of squares of the residuals, in the LAV method the sum of the absolute value of the residuals is minimized. Thus, the objective function is defined as

$$E = \sum_{i=1}^{n} \left| q_{meas,i} - q_{calc,i}(\vec{\alpha}, t_i) \right| \quad \text{.....(5.11)}$$

Therefore, starting by the equation of condition

$$q_{meas,i} = q_{calc,i}(\vec{\alpha}, t_i) \qquad i = 1, 2, \ldots, n \quad \text{.....(5.12)}$$

Expanding the model function using Taylor series around an initial guess, $\vec{\alpha}^0$, and considering only first order terms, we have

$$q_{meas,i} = q_{calc,i}(\vec{\alpha}^0, t_i) + (\alpha_1 - \alpha_1^0)\left[\frac{\partial q_{calc,i}(\vec{\alpha}, t_i)}{\partial \alpha_1}\right]_{\vec{\alpha}^0} + \ldots + (\alpha_{np} - \alpha_{np}^0)\left[\frac{\partial q_{calc,i}(\vec{\alpha}, t_i)}{\partial \alpha_{np}}\right]_{\vec{\alpha}^0} \quad \text{.....(5.13)}$$

Rearranging Eq. 5.13,

$$q_{meas,i} - q_{calc,i}(\vec{\alpha}^0, t_i) = (\alpha_1 - \alpha_1^0)\left[\frac{\partial q_{calc,i}(\vec{\alpha}, t_i)}{\partial \alpha_1}\right]_{\vec{\alpha}^0} + \ldots + (\alpha_{np} - \alpha_{np}^0)\left[\frac{\partial q_{calc,i}(\vec{\alpha}, t_i)}{\partial \alpha_{np}}\right]_{\vec{\alpha}^0} \quad \text{.....(5.14)}$$

Eq. 5.14 can be written as

$$w_i = \beta_1 v_{i,1} + \beta_2 v_{i,2} + \ldots + \beta_{np} v_{i,np} \quad \text{.....(5.15)}$$

where

$$w_i = q_{meas,i} - q_{calc,i}(\vec{\alpha}^0, t_i) \quad \text{.....(5.16)}$$

$$\beta_j = \alpha_j - \alpha_j^0 \quad \text{.....(5.17)}$$

and

$$v_{i,j} = \left[\frac{\partial q_{calc,i}(\vec{\alpha}, t_i)}{\partial \alpha_j} \right]_{\vec{\alpha}^0} \qquad i = 1,2,...,n \quad j = 1,2,...,np \quad \text{.....(5.18)}$$

Defining the right hand side of Eq. 5.15 as

$$\hat{w}_i = \beta_1 v_{i,1} + \beta_2 v_{i,2} + ... + \beta_{np} v_{i,np} \quad \text{.....(5.19)}$$

Now, the objective function becomes

$$E = \sum_{i=1}^{n} \left| w_i - \hat{w}_i \right| \quad \text{.....(5.20)}$$

The above system of equations (Eq. 5.15) is an overdetermined system with *n* equations and *np* unknowns. This system of equations is solved using *L1* Algorithm (Barrodale and Roberts 1974). The final solution is obtained iteratively following the procedures described in section 5.1 for the LS method. The two methods will be tested using synthetic and simulated data before they are applied to field cases as explained in the next sections

5.4 Regression Programming and Results

The triple-porosity solutions and the regression methods were programmed using Excel VBA along with a suite of other analytical solutions. The program is inherently called *Stehfest* (Stehfest 6A) since it uses Stehfest Algorithm (Stehfest 1970) to invert Laplace domain solutions to real time domain. Regression has been added as an independent module in this program.

The regression module reads the entire well and reservoir data for the triple-porosity model in addition to an initial guess for the designated unknown parameters. It

calculates the model response function, $q_{calc,i}(\vec{\alpha},t_i)$, using *Stehfest* program. Once a converged solution is obtained, the model is completely described. That is, all well and reservoir properties are known. Thus, calculations can be made such as original hydrocarbon in place (*OHIP*) and well's future performance forecasting.

5.5 Regression Testing Using Synthetic Data

In order to test the regression methods, a synthetic case is constructed using the triple-porosity fully transient model (Model 1). The input data for this case are shown in **Table 5.1**. The parameters that are assumed to be unknown are macro-fractures intrinsic permeability, $k_{F,in}$, micro-fractures intrinsic permeability, $k_{f,in}$, micro-fractures spacing, L_f, and drainage area half-width, y_e. The regression program is then used to estimate these parameters using least-squares and least absolute value methods.

The regression results are shown in **Table 5.2** and **Fig. 5.1**. Only the first 500 days of production were used in the regression. Both methods converged to the true solution. This confirms that the regression algorithm is working properly. The LS method takes less computational time as reflected on fewer iterations compared to the LAV method.

Table 5.1 – Input reservoir data for synthetic triple-porosity case					
φ_F		0.02	h	(ft)	300
$k_{F,in}$	(md)	1000	S_{wi}		0.29
w_F	(ft)	0.1	x_e	(ft)	2600
L_F	(ft)	130	y_e	(ft)	200
φ_f		0.01	p_i	(psi)	3000
$k_{f,in}$	(md)	1	p_{wf}	(psi)	500
w_f	(ft)	0.01	μ	(cp)	3.119
L_f	(ft)	20	B_o	(rbbl/STB)	1.05
φ_m		0.06	c_t	(psi^{-1})	3.39×10^{-6}
k_m	(md)	1.5×10^{-3}			

Table 5.2 – Regression results for the synthetic case				
	True Solution	First Guess	LS Results	LAV Results
$k_{F,in}$	1000	500	1000	1000
$k_{f,in}$	1	10	1	1
L_f	20	10	20	20
y_e	200	300	200	200
Iterations	–	–	15	16

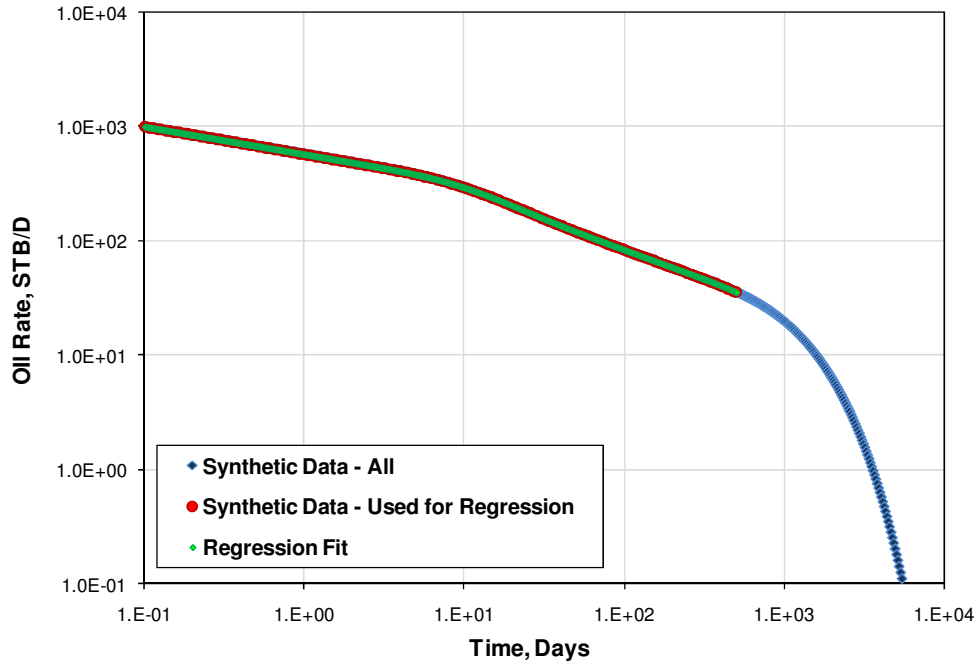

Fig. 5.1 – Regression results for the synthetic case using LS method. LV method results are identical and are not shown. The desired solution was achieved although not all data were used in regression.

5.6 Regression Testing Using Simulated Data

The synthetic case in 5.4 was generated using the same program that was used for regression. Although the match was obtained, it is necessary to test the regression program using data from a different source. Thus, the data in **Table 5.1** was used in CMG reservoir simulator to produce the same case. Regression results are shown in **Table 5.3** and **Fig. 5.2**.

Table 5.3 – Regression results for the simulated case				
	True Solution	First Guess	LS Results	LAV Results
$k_{F,in}$	1000	500	1863	2562
$k_{f,in}$	1	5	1.08	1.07
L_f	20	25	21.5	21.7
y_e	200	150	205	206
Iterations	–	–	7	8
OOIP	2,319,760		2,311,366	2,324,804

The regression results are matching for all parameters except the macro-fractures intrinsic permeability. Regression permeability is about two times the true value. This is due to the larger permeability in the macro-fractures which makes the transient flow in that system very fast and is not captured by the rate data. The simulation has to be run to report flow rate for very small fraction of a day in order to capture the flow in the macro-fractures.

The original oil in place for this case can be calculated by volumetric method. Both methods, however, gave excellent match of the *OOIP* since the estimated reservoir drainage area half-width, y_e, was very close to the true value.

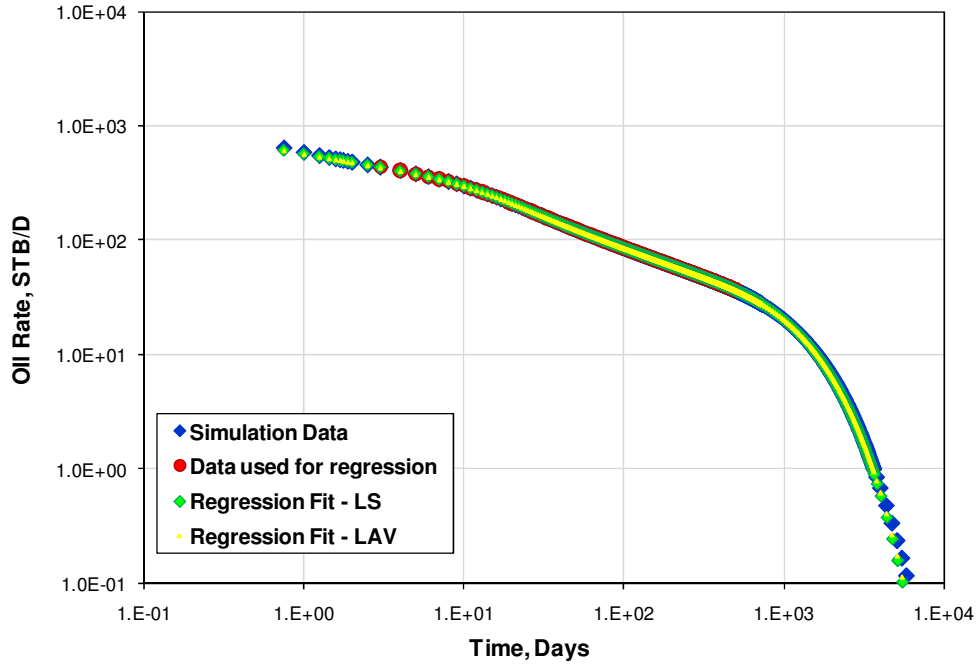

Fig. 5.2 – Regression results for the simulated case using LS and LAV methods. The match using both methods is almost identical. The solution was obtained without including all data in regression.

5.7 Matching Noisy Data

It is known that LS regression method is affected by outliers. Thus, some noise has been added to the synthetic data in section 5.5. The data was modified by changing the rate by10% and -5% every 5 pints alternatively. For example, the 5th point rate is increased by 10% while the 10th point rate was reduced by 5%.

The regression results are shown in **Table 5.4**. The LS method was affected by the noise and the computational time increased dramatically as it took 467 iterations to converge. The converged solution, however, is very close to the true solution.

The LAV, on the other hand, has not been affected by the noise. Thus, when dealing with field cases, the LAV method match will be honored.

Table 5.4 – Regression results for the synthetic noisy data				
	True Solution	First Guess	LS Results	LAV Results
$k_{F,in}$	1000	500	970	1000
$k_{f,in}$	1	10	1.07	1
L_f	20	10	19.9	20
y_e	200	300	196	200
Iterations	–	–	467	15

5.8 Matching Gas Wells Rate

Since the analytical solutions are originally derived for liquid flow, the regression algorithm was modified to account for changing gas properties in case of gas flow. This is achieved by using gas potential and normalized time instead of the time variable in calculating model response function. The procedure is similar to that proposed by Fraim and Wattenbarger (1987).

Fig. 5.3 shows a comparison of gas well rate match with and without using normalized time. As expected, the difference can be seen at later time once the boundary dominated flow begins.

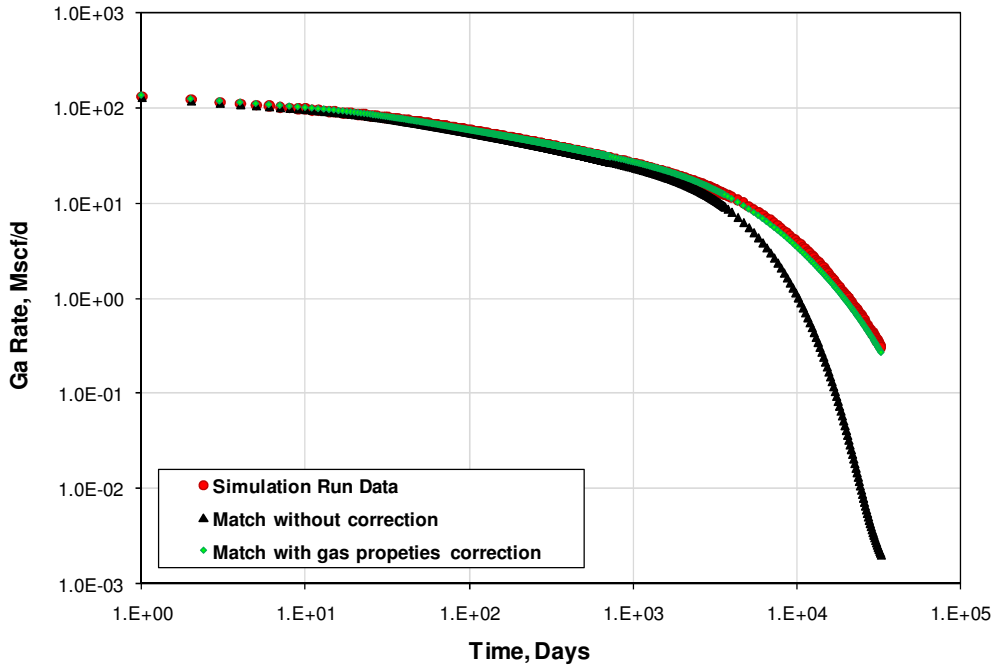

Fig. 5.3 – Effect of correcting for gas properties on matching gas flow case. The boundary dominated flow was matched very well after this modification.

5.9 Notes on Regression Matching

As described in Chapter III, the analytical solution may have more than one flow region. Therefore, in order to get the most accurate results with regression, data that shows special trends should be included in the regression. For example, if the data that shows linear flow was only included in the regression and the data that shows a bi-linear flow just before it was ignored, the data will be matched but the solutions will not be representative as if that data was also included. In short, the more data included in the regression, the more accurate the results will be.

CHAPTER VI

APPLICATION OF THE TRIPLE-POROSITY MODEL TO SHALE GAS WELLS

6.1 Introduction

Shale gas reservoirs play a major role in the United State natural gas supply as they are aggressively developed capitalizing on new technologies, namely horizontal wells with multi-stage fracturing. It has been observed that these wells behave as though they are controlled by transient linear flow (Bello 2009; Bello & Wattenbarger 2008, 2009, 2010; Al-Ahmadi *et al.* 2010). According to Medeiros *et al.* (2008) linear flow is the dominant flow regime for fractured horizontal wells in tight formations for most of their productive lives. This behavior is characterized by a negative half-slope on the log-log plot of gas rate versus time and a straight line on the $[m(p_i) - m(p_{wf})]/q_g$ vs. $t^{0.5}$ plot (the square-root of time plot).

Some shale gas wells, however, exhibit a bi-linear flow just before the linear flow is observed. This behavior is characterized by a negative quarter-slope on the log-log plot of gas rate versus time or a straight line on the $[m(p_i) - m(p_{wf})]/q_g$ vs. $t^{0.25}$ plot. The bi-linear flow is due to two perpendicular transient linear flows occurring simultaneously in two contiguous systems. These could be micro-fractures and matrix or micro-fractures and macro-fractures systems.

Previously, shale gas wells have been modeled using linear dual-porosity models (Bello 2009; Bello & Wattenbarger 2008, 2009, 2010; Al-Ahmadi *et al.* 2010). Dual-porosity idealizations are shown in **Fig. 6.1**.

In these models, the matrix was assumed to be "homogeneous" although it might be enhanced by natural fractures by having a high effective matrix permeability. In addition, orthogonal fractures are assumed to have identical properties. However, most if not all of horizontal wells drilled in shale gas reservoirs are hydraulically fractured. As the hydraulic fractures propagate, they re-activate the pre-existing natural fractures (Gale *et al.* 2007). The result will be two orthogonal fractures systems with different properties. Therefore, dual porosity model will not be sufficient to characterize these reservoirs.

As a result, the triple-porosity model with fully transient flow assumption (Model 1) will be used in this chapter to model horizontal shale gas wells. In this case, macro-fractures are the hydraulic fractures while micro-fractures are the natural fractures.

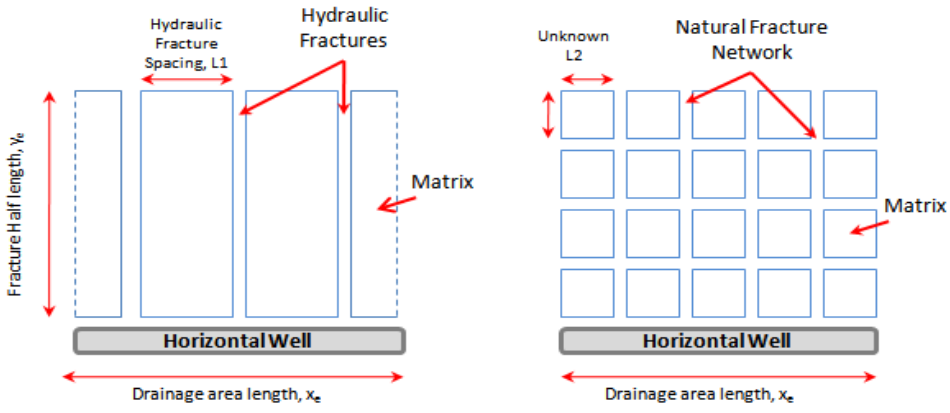

Fig. 6.1 – Dual-porosity models for shale gas horizontal wells: slab model on the left and cube model on the right (Al-Ahmadi *et al*. 2010).

6.2 Accounting for Adsorbed Gas

Unlike tight gas reservoirs, gas in shale reservoirs is stored as compressed (free) gas and adsorbed gas. Adsorbed gas does not usually flow until the pressure drops below the sorption pressure. Adsorbed gas can be accounted for using Langmuir isotherm which defines the adsorbed gas volume as

$$V = V_L \frac{p}{(p + p_L)} \quad \text{.....(6.1)}$$

where

V: Volume of gas currently adsorbed (scf/cuf)

V_L: Langmuir's volume (scf/cuf)

p_L: Langmuir's pressure (psia)

p: Reservoir pressure (psia)

Therefore, the analytical solutions have to account for the adsorbed gas before applying them to shale gas wells. This can be achieved by modifying the gas compressibility definition to include adsorbed gas. Following Bumb and McKee (1988), the modified total compressibility is defined as

$$c_t^* = c_f + (c_g + c_d) S_g + c_w S_w \quad \text{.....(6.2)}$$

where c_d is the desorbed gas compressibility given by

$$c_d = \frac{\rho_{g_{sc}} V_L p_L}{\varphi \bar{\rho}_g (p_L + \bar{p})^2} = \frac{B_g V_L p_L}{\varphi (p_L + \bar{p})^2} \quad \text{.....(6.3)}$$

Thus, to account for adsorption, c_t^* instead of c_t will be used in the analytical solutions to be applicable to shale gas wells.

For material balance calculations, the modified compressibility factor (z^*) is used instead of z (King 1993). z^* is defined as

$$z^* = \frac{z}{(1-S_{wi}) + \frac{V_L T\, p_{sc}\, z}{\varphi(p+p_L) T_{sc}\, z_{sc}}} \quad \text{.....(6.4)}$$

Then the gas material balance equation becomes

$$\frac{\overline{p}}{z^*} = \frac{p_i}{z_i^*}\left(1 - \frac{G_p}{G}\right) \quad \text{.....(6.5)}$$

The *OGIP* accounting for free and adsorbed gas can be calculated using the following volumetric equation (Mengal 2010)

$$G = V_b\left[\left(\frac{\varphi S_{gi}}{B_{gi}}\right) + \left(V_L \frac{p_i}{p_i + p_L}\right)\right] \quad \text{.....(6.6)}$$

6.3 Analysis Procedure

Due to the large number of variables involved in the triple-porosity model, non-linear regression will be utilized to estimate a set of unknown parameters by matching the well's production rate. Other parameters may be assumed or estimated through other methods. Including many variables in the regression may lead to non-uniqueness of the converged solution.

The parameters to be found by regression are fractures intrinsic permeabilities, drainage area half-width (hydraulic fracture half-length) and natural fractures spacing. After the match is obtained, the well model is fully defined. Hence, the *OGIP* can be calculated by volumetric method and well future production can be forecasted.

6.4 Field Cases

Two field cases from the Barnett Shale will be used to demonstrate the application of the triple-porosity model. Gas rate history for these wells is shown in **Fig. 6.2**. The fully transient model (Model 1) with non-linear regression and normalized time will be applied. Gas adsorption will be included in the analysis as well. The following adsorption data are used for the Barnett Shale (Mengal 2010):

V_L = 96 scf/ton

p_L = 650 psi

Bulk Density = 2.58 gm/cc

The wells are matched with the analytical solutions by first assuming no adsorbed gas and then including gas adsorption. Comparisons are made for each well.

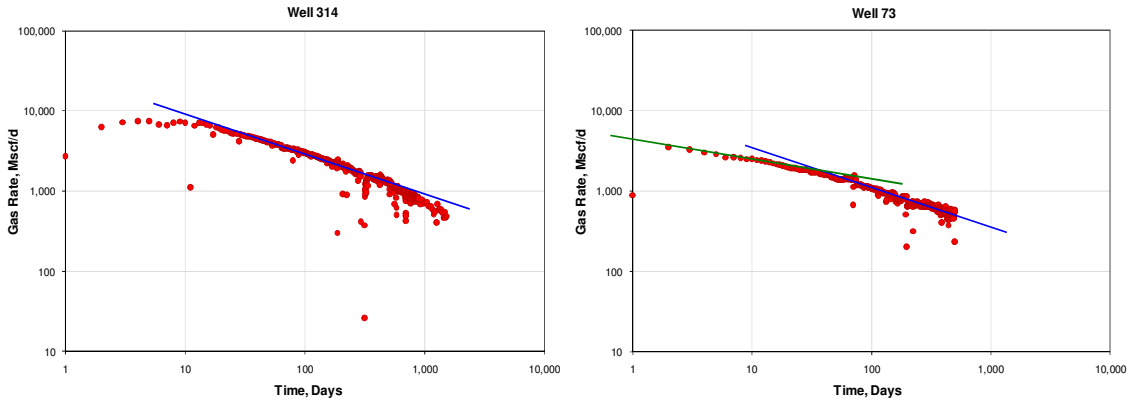

Fig. 6.2 – Log-Log plot of gas rate versus time for two horizontal shale gas wells. Well 314 exhibits a linear flow for almost two log cycles while Well 73 exhibit generally lower rate with bi-linear flow for early data and changed to linear flow at later time. The blue and green lines indicate a half-slope and a quarter-slope, respectively.

6.4.1 Well 314

Well 314 is a horizontal well with multi-stage hydraulic fracturing treatment producing at a constant bottom-hole pressure. The well production rate exhibits a half-slope on the log-log plot of rate versus time indicating a linear flow. However, the early and late data deviate from this trend. The early deviation may be due to skin effect due to the presence of fracturing job water in the hydraulic fractures making it difficult for the gas to start flowing to the well (Bello and Wattenbarger 2009; Al-Ahmadi *et al*. 2010). The later deviation is due to either start of boundary dominated flow (BDF) or reduction of well's drainage area due to drilling nearby well. In this work, no skin effect is considered and the later deviation will be dealt with as BDF. However, if the well is affected by skin, it results in a lower permeability value for the hydraulic fractures.

Table 6.1 summarizes well 314 data in addition to other assumed parameters. From the hydraulic fractures treatment, hydraulic fractures spacing is calculated assuming each perforation cluster corresponds to a hydraulic fracture. In addition, drainage area length, x_e, is the same as perforated interval. The matrix porosity and permeability used are the most available in the literature for the Barnett Shale. Representative values are assumed for fractures intrinsic porosity and width. Finally, the fractures intrinsic permeabilities, drainage area half-width and natural fractures spacing will be found by regression.

Regression results are shown in **Table 6.2** and **Fig. 6.3** with and without adsorption. Only LAV results are presented since the LS method did not produce a good match and took long computational time.

Table 6.1 – Well 314 data

"Known" Data			Assumed Data		
L_F	(ft)	106	φ_F		0.2
n_F		28	w_F	(ft)	0.1
φ_m		0.06	φ_f		0.01
k_m	(md)	1.5×10^{-4}	w_f	(ft)	0.01
h	(ft)	300			
x_e	(ft)	2968			
μ_{gi}	(cp)	0.0201	Unknown Data		
B_{gi}	(rcf/scf)	0.00509			
c_{ti}	(psi^{-1})	300×10^{-6}	$k_{F,in}$	(md)	
p_i	(psi)	2950	$k_{f,in}$	(md)	
p_{wf}	(psi)	500	y_e	(ft)	
$m(p_i)$	(psi^2/cp)	5.97×10^{8}	L_f	(ft)	
$m(p_{wf})$	(psi^2/cp)	2.03×10^{7}			
T	(°R)	610			
S_{wi}		0.3			

Table 6.2 – Regression results for Well 314

	First Guess	LAV Results (No Adsorption)	LAV Results (with Adsorption)
$k_{F,in}$	100	10.9	9.8
$k_{f,in}$	1	0.26	0.29
L_f	10	24	22.8
y_e	300	205	178
Iterations	–	18	57
OGIP, *Bscf*	–	3.01	4.64

From the regression results above, the hydraulic fractures intrinsic permeability is more than one order of magnitude compared to that of the natural fractures. In addition, the natural fractures permeability is about three orders of magnitude compared

to the matrix permeability. Furthermore, the natural fracture spacing is about 23 ft indicating that matrix is actually enhanced by natural fractures.

Including adsorption did not change the estimate of fractures intrinsic permeabilities or the natural fractures spacing but it had a big impact on drainage area half-width and consequently *OGIP*. Thus, including adsorption reduces the reservoir size while increasing its gas content by more than 50% noting that the same matrix porosity was used in both cases.

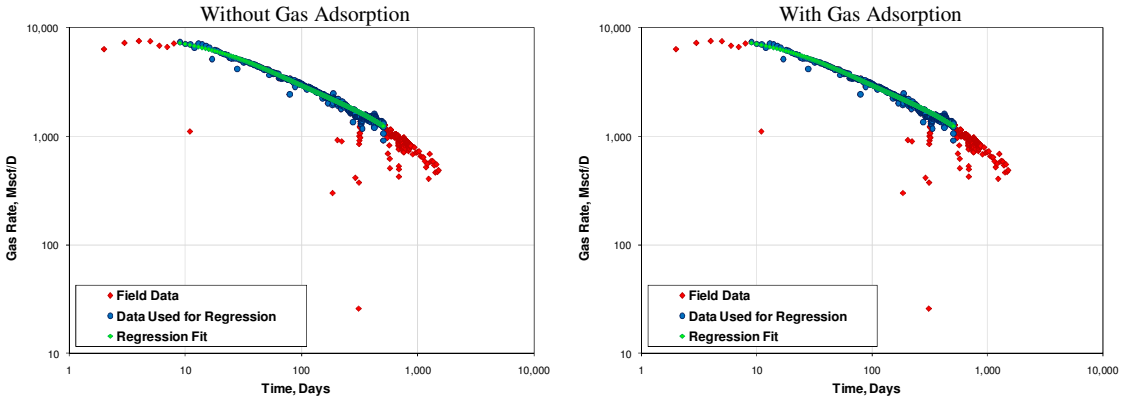

Fig. 6.3 – Regression results for Well 314. The left plot does not include gas adsorption while the right plot does. In both cases, the well's data was match using 500 days of production history.

The calculated *OGIP* is 3.01 *Bscf* if adsorbed gas is ignored. Al-Ahmadi *et al.* (2010) estimated 2.74 *Bscf* for *OGIP* for this well using linear dual-porosity model. The two estimates are within 10% relative error.

Knowing all the triple-porosity parameters, the whole well production history is forecasted as shown in **Fig. 6.4** based on the regression results for the first 500 days. As

can be seen, the model very well reproduced the well production trend with and without adsorption as shown on the log-log and decline curve plots.

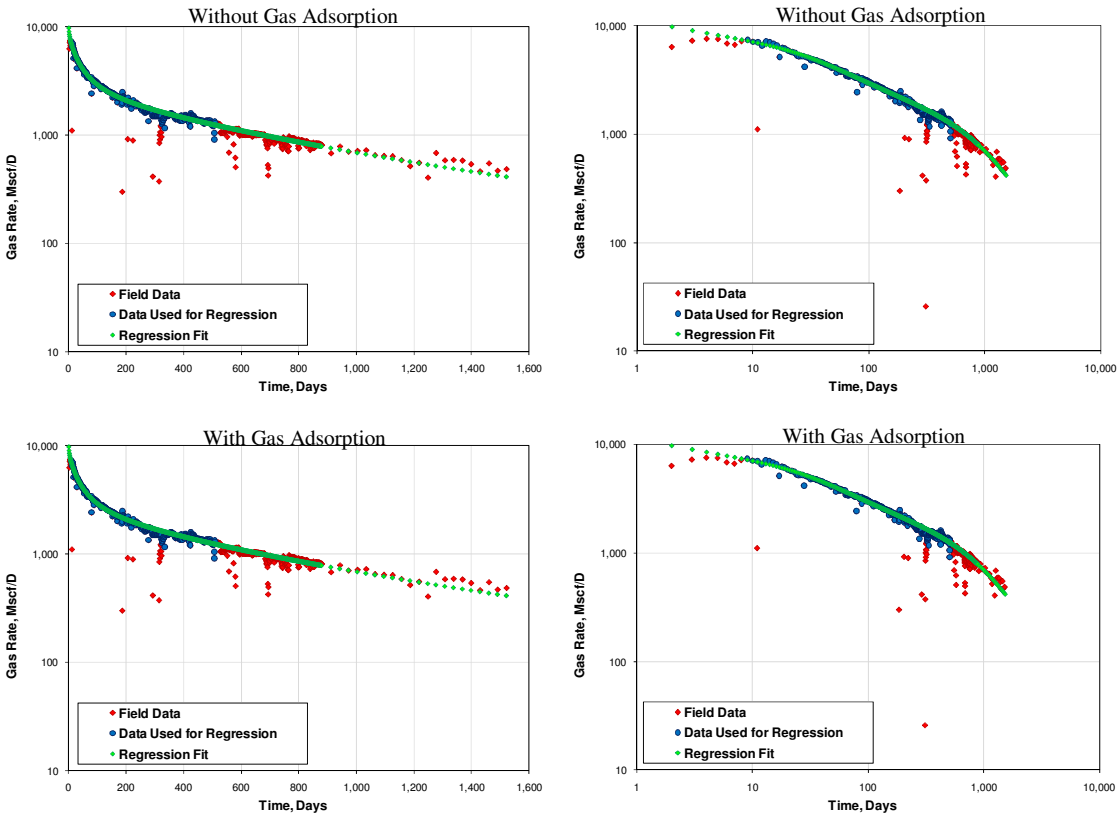

Fig. 6.4 – Matching Well 314 production history using the regression results with (bottom) and without (top) adsorption. On the left is the decline curve plot and log-log plot is on the right for gas rate vs. time.

6.4.2 Well 73

Well 73 is another horizontal well with multi-stage fractures treatment. Unlike Well 314, this well exhibits a bilinear for the first ten days followed by linear flow. No boundary dominated flow is observed. The well data is shown in **Table 6.3**.

All rate data were used for regression since no good match was obtained using fewer data points. The regression results are shown in **Table 6.4** and **Fig. 6.5**. As the case with Well 314, LAV regression method was used. As can be seen in **Fig. 6.5**, the regression match described the well trend perfectly with and without gas adsorption.

Table 6.3 – Well 73 data

"Known" Data			Assumed Data		
L_F	(ft)	79	φ_F		0.2
n_F		18	w_F	(ft)	0.1
φ_m		0.06	φ_f		0.01
k_m	(md)	1.5×10^{-4}	w_f	(ft)	0.01
h	(ft)	300			
x_e	(ft)	1420			
μ_{gi}	(cp)	0.0201	Unknown Data		
B_{gi}	(rcf/scf)	0.00509			
c_{ti}	(psi^{-1})	300×10^{-6}	$k_{F,in}$	(md)	
p_i	(psi)	2950	$k_{f,in}$	(md)	
p_{wf}	(psi)	500	y_e	(ft)	
$m(p_i)$	(psi^2/cp)	5.97×10^{8}	L_f	(ft)	
$m(p_{wf})$	(psi^2/cp)	2.03×10^{7}			
T	(°R)	610			
S_{wi}		0.3			

Table 6.4 – Regression results for Well 73

	First Guess	LAV Results (No Adsorption)	LAV Results (with Adsorption)
$k_{F,in}$	10	3.7	3.3
$k_{f,in}$	0.5	0.1	0.11
L_f	15	23	22
y_e	250	185	163
Iterations	–	13	13
OGIP, *Bscf*	–	1.32	2.05

As shown in **Table 6.4**, the regression results are almost the same with and without adsorption except for y_e. The *OGIP* increased significantly when adsorption is included.

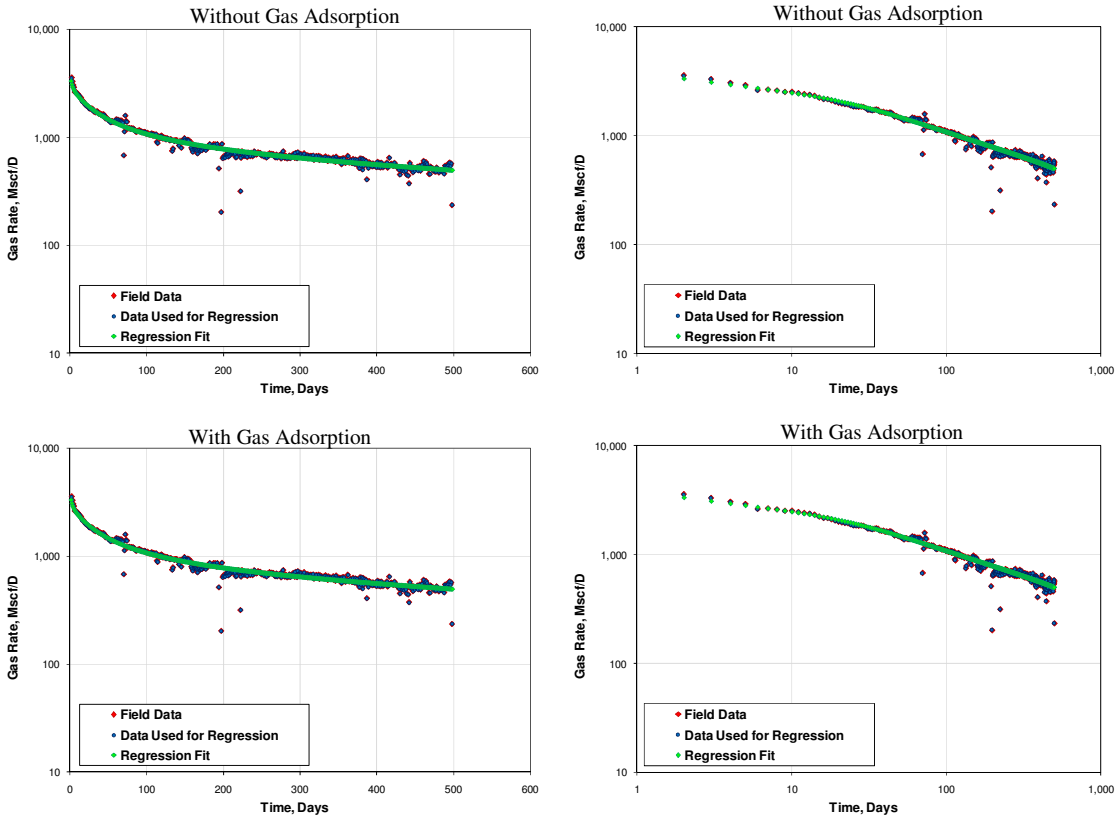

Fig. 6.5 – Regression match for Well 73 where it described the well trend perfectly with (bottom) and without (top) gas adsorption. No good match was obtained unless the whole data is used in the regression. On the left is the decline curve plot and log-log plot is on the right for gas rate vs. time.

6.5 Effect of Outer Reservoir

In shale gas wells analysis, it is common that the stimulated reservoir volume (SRV) is only considered. It is believed that the outer reservoir, the area beyond the hydraulic fractures tip, does not contribute much to the well production (Mayerhofer *et*

al. 2006). Ozkan *et al*. (2009) also concluded that outer reservoir contribution is technically outside the practical life-span of the well.

However, Anderson *et al*. (2010) demonstrated that outer reservoir contribution might be significant depending on how large is the matrix permeability which determines when outer reservoir effect starts. Thus, the well may exhibit a short boundary dominated flow followed by an infinite acting flow.

Therefore, a simulation run was made for a gas well with typical Barnett Shale data using the triple-porosity simulation model. 400' of outer reservoir has been added that has matrix permeably similar to that in the SRV. The outer reservoir added to the simulation model is shown schematically in **Fig. 6.6**.

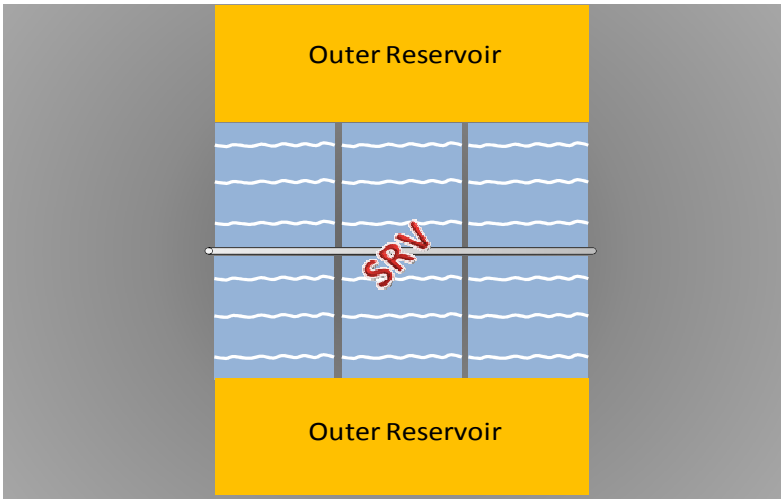

Fig. 6.6 – A sketch of the outer reservoir considered in the simulation model.

The simulation results are shown in **Fig. 6.7**. From the rate comparison, the outer reservoir contribution is becoming significant after four years of production. If the reservoir matrix permeability if very small, this effect will be delayed. However, if there

are natural fractures present in this section enhancing its permeability, the effect will be more pronounced and will be significant earlier in well life.

Although triple-porosity model is used to analyze the SRV performance, it does not account for the outer reservoir contribution. Nonetheless, this behavior has not been observed in any field case yet.

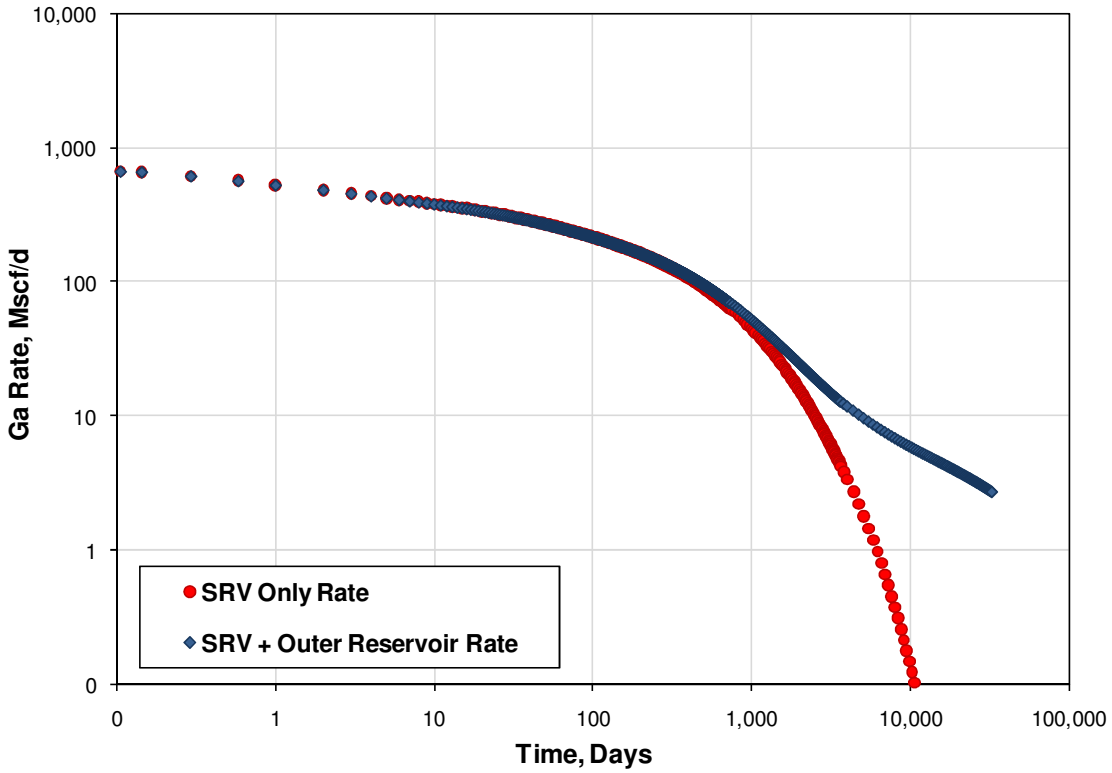

Fig. 6.7 – Comparison of a gas well rate showing the effect of outer reservoir. The outer reservoir effect is significant after four years of production for this set of data. Only free gas is considered for this case.

6.6 Chapter Summary

Triple-porosity Model 1 was applied to shale gas wells. Gas adsorption was incorporated in the model. The model successfully matched well production rate using the non-linear regression with and without gas adsorption. When adsorbed gas is included, it resulted in a smaller reservoir size but the *OGIP* is increased noticeably.

CHAPTER VII

CONCLUSIONS AND RECOMMENDATIONS

7.1 Conclusions

The major conclusions from this work can be summarized as follows:

1. New triple-porosity (dual-fracture) solutions have been developed for fractured linear reservoirs.
2. Six flow regions can be identified for fully transient triple-porosity model (Model 1)
3. The new model has been verified by reducing it to simpler models such as dual and single (homogeneous) porosity models and by comparing it to reservoir simulation.
4. The newly derived fracture functions are applicable to radial flow.
5. The derived solutions are also applicable to gas flow using gas potential and normalized time.
6. Least absolute value regression method proves to be robust in matching noisy data and can be used effectively with triple-porosity model to match field data.
7. Triple-porosity fully transient model (Model 1) is applicable to fractured shale gas horizontal wells when gas adsorption is incorporated. The model can be used to match field data, characterize well drainage area, determine reservoir size and OGIP and forecast future production.

7.2 Recommendations

The followings can be recommended to add to the usefulness of this work:

1. The triple-porosity model was derived for sequential flow. Thus, other flow combinations such as simultaneous flow may worth investigation.
2. Including skin factor in the regression variables.
3. Development of analysis equation for each flow region and use that for analyzing well performance. More properties will be estimated from each region than using regression to match the whole well history.
4. Using derivative analysis to identify each flow region accurately.
5. Using superposition with respect to time to model variable rate and variable bottom-hole pressure cases.

NOMENCLATURE

A_{cw}	cross-sectional area to flow defined as $2hx_e$, ft^2
A_{cm}	total matrix surface area draining into fracture system, ft^2
B_{gi}	formation volume factor at initial reservoir pressure, rcf/scf
c_t	total compressibility, psi^{-1}
E	objective function
$\vec{g}$	objective function gradient
h	reservoir thickness, ft
H	Hessian matrix
k_F	macro-fractures bulk permeability, md
k_f	micro-fracture bulk permeability, md
$k_{F,in}$	macro-fracture intrinsic permeability, md
$k_{f,in}$	micro-fracture intrinsic permeability, md
k_m	matrix permeability, md
L_F	macro-fractures spacing, ft
L_f	micro-fractures spacing, ft
$m(p)$	pseudopressure (gas), psi^2/cp
p_D	dimensionless pressure (transient triple porosity model)
p_i	initial reservoir pressure, psi
p_{wf}	wellbore flowing pressure, psi
q_D	dimensionless rate (transient triple porosity model)

q_{DL}	dimensionless rate based on $A_{cw}^{0.5}$ and k_F (rectangular geometry, triple porosity)
q_g	gas rate, Mscf/day
r_w	wellbore radius, ft
S_{gi}	initial gas saturation, fraction
S_{wi}	initial water saturation, fraction
T	absolute temperature, ^{o}R
t	time, days
t_{DAcw}	dimensionless time based on A_{cw} and k_F (rectangular geometry, triple-porosity)
t_{esr}	time to end of straight line on the square root of time plot, days
V_b	total system bulk volume, ft^3
V	bulk volume fraction, dimensionless
x_e	drainage area length (rectangular geometry), ft
y_{De}	dimensionless reservoir half-width (rectangular geometry)
y_e	drainage area half-width (rectangular geometry), equivalent to fracture half-length, ft

Greek symbols

α	Warren & Root shape factor
$\vec{\alpha}$	vector of unknown regression parameters
λ	dimensionless interporosity parameter

μ	viscosity, cp
ω	dimensionless storativity ratio
φ	porosity

Subscripts

i	initial
F	macro-fracture (hydraulic fracture)
f	micro-fracture (natural fracture)
m	matrix
$t = F+f+m$	total system (macro-fracture +micro-fracture + matrix)

Superscripts

$\bar{x}$	Laplace transform of variable x
x^k	k^{th} iteration of variable x
$\vec{x}^T$	transpose of vector $\vec{x}$

REFERENCES

Abdassah, D. and Ershaghi, I. 1986. Triple-Porosity Systems for Representing Naturally Fractured Reservoirs. *SPE Form Eval* (April): 113 – 127. SPE-13409-PA.

Al-Ahmadi, H. A., Almarzooq, A. M. and Wattenbarger, R. A. 2010. Application of Linear Flow Analysis to Shale Gas Wells – Field Cases. Paper SPE 130370 presented at the 2010 Unconventional Gas Conference, Pittsburgh, Pennsylvania, 23 – 25 February.

Al-Ghamdi, A. and Ershaghi, I. 1996. Pressure Transient Analysis of Dually Fractured Reservoirs. *SPE J.* (March): 93 – 100. SPE-26959-PA.

Al-Hussainy, R., Ramey, H. J., Jr., and Crawford, P. B. 1966. The Flow of Real Gas Through Porous Media. *J. Pet Tech* (May): 624 – 636. SPE-1243A-PA

Anderson, D. M., Nobakht, M., Moghadam, S. and Mattar, L. 2010. Analysis of Production Data from Fractured Shale Gas Wells. Paper SPE 131787 presented at the SPE Unconventional Gas Conference, Pittsburgh, Pennsylvania, 23 – 25 February.

Barenblatt, G. I., Zhelto, I. P. and Kochina, I. N. 1960. Basic Concepts of the Theory of Seepage of Homogeneous Liquids in Fissured Rocks. *Journal of Applied Mathematical Mechanics* (USSR) **24** (5): 852 – 864.

Barrodale, I. and Roberts, F. D. K. 1974. Solution of an Overdetermined System of Equations in the l_1 Norm. *Communication of the ACM* **17** (6): 319 – 320.

Bello, R.O. 2009. Rate Transient Analysis in Shale Gas Reservoirs with Transient Linear Behavior. Ph.D. Dissertation, Texas A&M U., College Station, Texas.

Bello, R. O. and Wattenbarger, R. A. 2008. Rate Transient Analysis in Naturally Fractured Shale Gas Reservoirs. Paper SPE 114591 presented at the CIPC/SPE Gas Technology Symposium 2008 Joint Conference, Calgary, Alberta, Canada, 16 – 19 June.

Bello, R. O. and Wattenbarger, R. A. 2009. Modeling and Analysis of Shale Gas Production with a Skin Effect. Paper CIPC 2009-082 presented at the Canadian International Petroleum Conference, Calgary, Alberta, Canada, 16 – 18 June.

Bello, R. O. and Wattenbarger, R. A. 2010. Multi-stage Hydraulically Fractured Shale Gas Rate Transient Analysis. Paper SPE 126754 presented at the SPE North Africa Technical Conference and Exhibition held in Cairo, Egypt, 14 – 17 February.

Brown, M., Ozkan, E., Raghavan, R. and Kazemi, H. 2009. Practical Solutions for Pressure Transient Responses of Fractured Horizontal Wells in Unconventional Reservoirs. Paper SPE 125043 presented at the Annual Technical Conference and Exhibition, New Orleans, Louisiana, 4 – 7 October.

Bumb, A. C and McKee, C. R. 1988. Gas-Well Testing in the Pressure of Desorption for Coalbed Methane and Devonian Shale. *SPE Form Eval* (March): 179 - 185. SPE-15227-PA.

Cheney, E.W. and Kincaid, R. D. 1985. Numerical Mathematics and Computing, 2nd edition. Monterey, California: Brooks/Cole Publishing Company.

de Swaan, O. A. 1976. Analytic Solutions for Determining Naturally Fractured Reservoir Properties by Well Testing. *SPE J.* (June): 117 – 122. SPE-5346-PA.

Dreier, J. 2004. Pressure-Transient Analysis of Wells in Reservoirs with a Multiple Fracture Network. M.Sc. Thesis, Colorado School of Mines, Golden, Colorado.

Dreier, J., Ozkan, E. and Kazemi, H. 2004. New Analytical Pressure-Transient Models to Detect and Characterize Reservoirs with Multiple Fracture Systems. Paper SPE 92039 presented at the SPE International Petroleum Conference in Mexico, Puebla, Mexico, 8 – 9 November.

El-Banbi, A.H. 1998. Analysis of Tight Gas Wells. Ph.D. Dissertation, Texas A &M U., College Station, Texas.

Fraim, M. L. and Wattenbarger, R. A. 1987. Gas Reservoir Decline-Curve Analysis Using Type Curve with Real Gas Pseudopressure and Normalized Time. *SPE Form Eval* (December): 671 – 682. SPE-14238-PA.

Gale, J. F., Reed, R. M. and Holder, J. 2007. Natural Fractures in the Barnett Shale and Their Importance for Hydraulic Fracture Treatments. *AAPG Bulletin*. **91** (4): 603 – 622.

Jalali, Y. and Ershaghi, I. 1987. Pressure Transient Analysis of Heterogeneous Naturally Fractured Reservoirs. Paper SPE 16341 presented at the SPE California Regional Meeting, Ventura, California, 8 – 10 April.

Kazemi, H. 1969. Pressure Transient of Naturally Fractured Reservoirs with Uniform Fracture Distribution. *SPE J.* (December):451– 462. SPE-2156A-PA.

King, G. R. 1993. Material-Balance Techniques for Coal-Seam and Devonian Shale Gas Reservoirs with Limited Water Influx. *SPE Res Eng* (February): 67 – 72. SPE-20730-PA.

Liu, C. Q. 1981. Exact Solution for the Compressible Flow Equations through a Medium with Triple-Porosity. *Applied Mathematics and Mechanics* **2** (4): 457 – 462.

Liu, C. Q. 1983. Exact Solution of Unsteady Axisymmetrical Two-Dimensional Flow through Triple Porous Media. *Applied Mathematics and Mechanics* **4** (5): 717 – 724.

Liu, J. C., Bodvarsson, G. S. and Wu, Y. S. 2003. Analysis of Flow Behavior in Fractured Lithophysal Reservoirs. *Journal of Contaminant Hydrology* **62-63**: 189 – 211.

Mayerhofer, M. J., Lolon, E. P., Youngblood, J. E. and Heinze, J. R. 2006. Integration of Microseismic Fracture Mapping Results with Numerical Fracture Network Production Modeling in the Barnett Shale. Paper SPE 102103 presented at the Annual Technical Conference and Exhibition, San Antonio, Texas, 24 – 27 September.

Medeiros, F., Ozkan, E. and Kazemi, H. 2008. Productivity and Drainage Area of Fractured Horizontal Wells in Tight Gas Reservoirs. *SPE Res Eval & Eng* (October): 902 – 911. SPE-108110-PA.

Mengal, S. A. 2010. Accounting for Adsorbed Gas and Its Effect on Production Behavior of Shale Gas Reservoirs. M.Sc. Thesis, Texas A&M U., College Station, Texas.

Nelson, R. A. 2001. Geologic Analysis of Naturally Fractured Reservoirs, 2nd edition. Woburn, Massachusetts: Butterworth-Heinemann.

Ozkan, E., Brown, M., Raghavan, R. and Kazemi, H. 2009. Comparison of Fractured Horizontal-Well Performance in Conventional and Unconventional Reservoirs. Paper SPE 121290 presented at the SPE Western Regional Meeting, San Jose, California, 24 – 26 March.

Ozkan, E., Ohaeri, U. and Raghavan, R. 1987. Unsteady Flow to a Well Produced at a Constant Pressure in Fractured Reservoir. *SPE Form Eval* (June): 186 - 200. SPE-9902-PA.

Rosa, A. J. and Horne, R. N. 1995. Automated Well Test Analysis Using Robust (LAV) Nonlinear Parameter Estimation. *SPE Advanced Technology Series* **3** (1): 95 – 102. SPE-22679-PA.

Rosa, A. J. and Horne, R. N. 1996. New Approaches for Robust Nonlinear Parameter Estimation in Automated Well Test Analysis Using the Least Absolute Value Criterion. *SPE Advanced Technology Series* **4** (1): 21 – 27. SPE-26964-PA.

Sarma, P. and Aziz, K. 2006. New Transfer Functions for Simulation of Naturally Fractured Reservoirs with Dual-Porosity Models. *SPE J.* (September): 328 – 340. SPE-90231-PA.

Stehfest, H. 1970. Algorithm 358 – Numerical Inversion of Laplace Transforms. *Communication of the ACM* **13** (1): 47 – 49.

Van Everdingen, A. F. and Hurst, W. 1949. The Application of the Laplace Transformation to Flow Problems in Reservoirs. *Trans.*, AIME, **186:** 305 – 324.

Warren, J. E. and Root, P. J. 1963. The Behavior of Naturally Fractured Reservoirs. *SPE J.* (September): 245 – 255. SPE-426-PA.

Wattenbarger, R.A. 2007. Some Reservoir Performance Aspects of Unconventional Gas Production. Private Conference Presentation, Lake Louise, Alberta, Canada.

Wu, Y. S., Liu, H. H. and Bodvarsson, G. S. 2004. A Triple-Continuum Approach for Modeling Flow and Transport Processes in Fractured Rock. *Journal of Contaminant Hydrology* **73**: 145 – 179.

APPENDIX A

LINEAR FLOW SOLUTIONS FOR FRACTURED LINEAR RESERVOIRS

Laplace transformation with respect to dimensionless time, t_{DAc}, is used to derive the rate solutions in fractured reservoirs. This transformation enables us to reduce the second-order partial differential flow equation to a second-order ordinary differential equation in Laplace domain. The solution is then easy to obtain in Laplace domain which can be inverted to time domain using Stehfest algorithm (Stehfest 1970).

Upon transformation, the differential equation in Laplace domain that describes the main flow in linear reservoir system shown in **Fig. A-1** is given by

$$\frac{\partial^2 \overline{p_{DLF}}}{\partial y_D^2} - s\, f(s)\, \overline{p_{DLF}} = 0 \quad \text{.....(A-1)}$$

This form of equation makes it easy to solve for different fractured reservoirs with varying degree of complexity by having different fracture function, $f(s)$. For the simplest case, i.e., homogeneous reservoir, $f(s)=1$. s in Eq. A-1 is the Laplace transform parameter.

Linear flow solutions for fractured linear reservoirs assuming dual-porosity system was first developed by El-Banbi (1998).

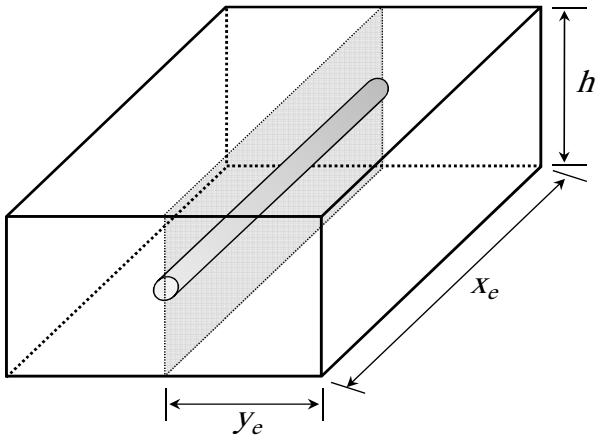

Fig. A-1 – A sketch of a horizontal well in a rectangular reservoir. Linear flow is the main flow regime.

A-1 Constant Rate Solution

For a closed linear reservoir, Eq. A-1 is subject to the following initial and boundary conditions:

Initial condition: $\overline{p_{DLF}}(y_D,0)=0$

Inner boundary: $\left.\dfrac{\partial \overline{p_{DLF}}}{\partial y_D}\right|_{y_D=0}=\dfrac{-2\pi}{s}$ (Constant Rate)

Outer boundary: $\dfrac{\partial \overline{p_{DLF}}}{\partial y_D}=0$ @ $y_D=y_{De}=y_e/\sqrt{A_{cw}}$ (No Flow Boundary)

The general solution for Eq. A-1 is given by

$$\overline{p_{DLF}}=A\cosh\left(\sqrt{s\,f(s)}\,y_D\right)+B\sinh\left(\sqrt{s\,f(s)}\,y_D\right) \quad \text{.....(A-2)}$$

The constants A and B are determined as:

1. At $y_D = 0$:

$$\frac{\partial \overline{p_{DLF}}}{\partial y_D} = A\sqrt{s\,f(s)}\,\sinh\left(\sqrt{s\,f(s)}\,y_D\right) + B\sqrt{s\,f(s)}\,\cosh\left(\sqrt{s\,f(s)}\,y_D\right) \quad \text{.....(A-3)}$$

$$-\frac{2\pi}{s} = B\sqrt{s\,f(s)} \quad \text{.....(A-4)}$$

Thus,

$$B = -\frac{2\pi}{s\sqrt{s\,f(s)}} \quad \text{.....(A-5)}$$

2. At $y_D = y_{De}$:

$$\frac{\partial \overline{p_{DLF}}}{\partial y_D} = A\sqrt{s\,f(s)}\,\sinh\left(\sqrt{s\,f(s)}\,y_D\right) - \frac{2\pi}{s}\,\cosh\left(\sqrt{s\,f(s)}\,y_D\right) \quad \text{.....(A-6)}$$

$$A\sqrt{s\,f_F(s)}\,\sinh\left(\sqrt{s\,f(s)}\,y_{De}\right) - \frac{2\pi}{s}\,\cosh\left(\sqrt{s\,f(s)}\,y_{De}\right) = 0 \quad \text{.....(A-7)}$$

Thus,

$$A = \frac{2\pi}{s\sqrt{s\,f(s)}}\,\frac{\cosh\left(\sqrt{s\,f(s)}\,y_{De}\right)}{\sinh\left(\sqrt{s\,f(s)}\,y_{De}\right)} \quad \text{.....(A-8)}$$

Therefore, Eq. A-2 now becomes

$$\overline{p_{DLF}} = \frac{2\pi}{s\sqrt{s\,f(s)}}\,\frac{\cosh\left(\sqrt{s\,f(s)}\,y_{De}\right)}{\sinh\left(\sqrt{s\,f(s)}\,y_{De}\right)}\cosh\left(\sqrt{s\,f_F(s)}\,y_D\right) - \frac{2\pi}{s\sqrt{s\,f(s)}}\sinh\left(\sqrt{s\,f(s)}\,y_D\right)$$

.....(A-9)

Applying Eq. A-9 at the well ($y_D = 0$), the constant rate solution becomes

$$\overline{p_{wDL}} = \frac{2\pi}{s\sqrt{s\,f(s)}}\,\frac{\cosh\left(\sqrt{s\,f(s)}\,y_{De}\right)}{\sinh\left(\sqrt{s\,f(s)}\,y_{De}\right)} \quad \text{.....(A-10)}$$

Upon Algebraic manipulations of Eq. A-10 (El-Banbi 1998; Bello 2009)

$$\overline{\overline{p_{wDL}}} = \frac{2\pi}{s\sqrt{s\,f(s)}}\left[\frac{1+\exp\left(-2\sqrt{s\,f(s)}\,y_{De}\right)}{1-\exp\left(-2\sqrt{s\,f(s)}\,y_{De}\right)}\right] \quad \text{.....(A-11)}$$

A-2 Constant Pressure Solution

In Laplace domain, the constant rate and constant pressure solutions at the wellbore are related by Eq. A-12 (Van Everdingen and Hurst 1949)

$$\overline{\overline{p_{wDL}}} \times \overline{q_{DL}} = \frac{1}{s^2} \quad \text{.....(A-12)}$$

Therefore, the solution for constant pressure case (El-Banbi 1998) is

$$\frac{1}{\overline{\overline{q_{DL}}}} = \frac{2\pi s}{\sqrt{s\,f(s)}}\left[\frac{1+\exp\left(-2\sqrt{s\,f(s)}\,y_{De}\right)}{1-\exp\left(-2\sqrt{s\,f(s)}\,y_{De}\right)}\right] \quad \text{.....(A-13)}$$

In subsequent appendixes, different fracture functions, $f(s)$, are derived. The above solutions are then used to get the final solution.

A-3 Accounting for Wellbore Storage and Skin

Once the fracture function, $f(s)$, is derived for the case without skin and wellbore storage effects, El-Banbi's solutions that account for these effects can be used. These solutions are already programmed in the *Stehfest* VBA program. Refer to El-Banbi Dissertation (El-Banbi 1998) for complete list of solutions.

APPENDIX B

DERIVATION OF LINEAR TRIPLE-POROSITY ANALYTICAL SOLUTION FOR FULLY TRANSIENT FLUID TRANSFER – MODEL 1

A simple sketch of the triple-porosity (dual-fracture) system is shown in **Fig. B-1**. The assumption is that the flow is sequential. That is, it is from matrix to micro-fractures to the macro-fractures and then to the well.

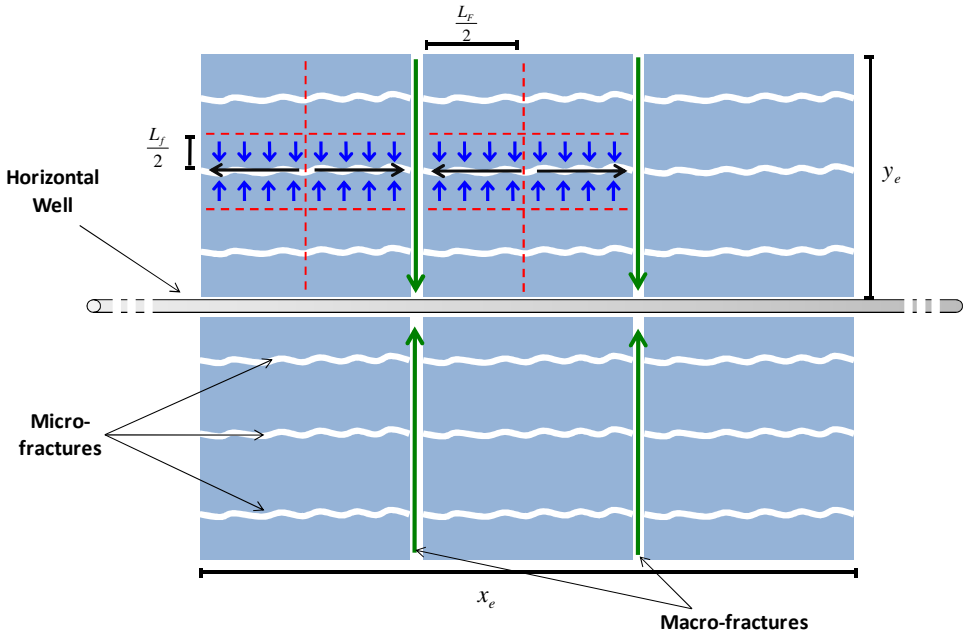

Fig. B-1 – A sketch of triple-porosity system under sequential feed assumption. Arrows show flow directions.

B-1 Matrix Equation

Since the flow transfer from matrix to fractures is under transient condition, the matrix equation is given by:

$$\frac{k_m}{\mu}\frac{\partial^2 p_m}{\partial z^2} = (\varphi V c_t)_m \frac{\partial p_m}{\partial t} \quad \text{.....(B-1)}$$

Or

$$\frac{\partial^2 p_m}{\partial z^2} = \frac{[\varphi V \mu c_t]_m}{k_m}\frac{\partial p_m}{\partial t} \quad \text{.....(B-2)}$$

Note: z here is a direction parallel to y-axis. It is not the vertical direction.

B-2 Micro-fracture Equation

$$\frac{k_f}{\mu}\frac{\partial^2 p_f}{\partial x^2} + q_{source,m} = (\varphi V c_t)_f \frac{\partial p_f}{\partial t} \quad \text{.....(B-3)}$$

$q_{source,m}$ is a source term of flow from matrix to the micro-fracture under transient flow and can be written as

$$q_{source,m} = -\frac{1}{L_f/2}\frac{k_m}{\mu}\frac{\partial p_m}{\partial z}\bigg|_{z=L_f/2} \quad \text{.....(B-4)}$$

Thus, the final form of micro-fractures equation is

$$\frac{k_f}{\mu}\frac{\partial^2 p_f}{\partial x^2} = (\varphi V c_t)_f \frac{\partial p_f}{\partial t} + \frac{1}{L_f/2}\frac{k_m}{\mu}\frac{\partial p_m}{\partial z}\bigg|_{z=L_f/2} \quad \text{.....(B-5)}$$

$$\frac{\partial^2 p_f}{\partial x^2} = \frac{[\varphi V \mu c_t]_f}{k_f}\frac{\partial p_f}{\partial t} + \frac{1}{L_f/2}\frac{k_m}{k_f}\frac{\partial p_m}{\partial z}\bigg|_{z=L_f/2} \quad \text{.....(B-6)}$$

B-3 Macro-fracture Equation

The macro-fractures receives flow from the micro-fractures and the flow can be modeled using the equation

$$\frac{k_F}{\mu}\frac{\partial^2 p_F}{\partial y^2} + q_{source,f} = (\varphi V c_t)_F \frac{\partial p_F}{\partial t} \quad \text{.....(B-7)}$$

$q_{source,f}$ is the source term of flow from micro-fractures to the macro-fracture under transient flow and can be written as

$$q_{source,f} = -\frac{1}{L_F/2}\frac{k_f}{\mu}\frac{\partial p_f}{\partial x}\bigg|_{x=L_F/2} \quad \text{.....(B-8)}$$

Thus, the final form of micro-fractures equation is

$$\frac{k_F}{\mu}\frac{\partial^2 p_F}{\partial y^2} = (\varphi V c_t)_F \frac{\partial p_F}{\partial t} + \frac{1}{L_F/2}\frac{k_f}{\mu}\frac{\partial p_f}{\partial x}\bigg|_{x=L_F/2} \quad \text{.....(B-9)}$$

$$\frac{\partial^2 p_F}{\partial y^2} = \frac{[\varphi V \mu c_t]_F}{k_F}\frac{\partial p_F}{\partial t} + \frac{1}{L_F/2}\frac{k_f}{k_F}\frac{\partial p_f}{\partial x}\bigg|_{x=L_F/2} \quad \text{.....(B-10)}$$

B-4 System of Equations with Initial and Boundary Conditions

Matrix: $$\frac{\partial^2 p_m}{\partial z^2} = \frac{[\varphi V \mu c_t]_m}{k_m}\frac{\partial p_m}{\partial t} \quad \text{.....(B-2)}$$

Micro-fractures: $$\frac{\partial^2 p_f}{\partial x^2} = \frac{[\varphi V \mu c_t]_f}{k_f}\frac{\partial p_f}{\partial t} + \frac{1}{L_f/2}\frac{k_m}{k_f}\frac{\partial p_m}{\partial z}\bigg|_{z=L_f/2} \quad \text{.....(B-6)}$$

Macro-fractures: $$\frac{\partial^2 p_F}{\partial y^2} = \frac{[\varphi V \mu c_t]_F}{k_F}\frac{\partial p_F}{\partial t} + \frac{1}{L_F/2}\frac{k_f}{k_F}\frac{\partial p_f}{\partial x}\bigg|_{x=L_F/2} \quad \text{.....(B-10)}$$

Initial and boundary conditions are:

Matrix:

Initial condition: $p_m(z,0) = p_i$

Inner boundary: $\frac{\partial p_m}{\partial z} = 0 \qquad @ \quad z = 0$

Outer boundary: $p_m = p_f \qquad @ \quad z = \frac{L_f}{2}$

Micro-fractures:

Initial condition: $p_f(x,0) = p_i$

Inner boundary: $\frac{\partial p_f}{\partial x} = 0 \qquad @ \quad x = 0$

Outer boundary: $p_f = p_F \qquad @ \quad x = \frac{L_F}{2}$

Macro-fractures:

Initial condition: $p_F(y,0) = p_i$

Inner boundary: $q = -\frac{k_F A_{cw}}{\mu} \frac{\partial p_F}{\partial y}\Big|_{y=0}$

Outer boundary: $\frac{\partial p_F}{\partial y} = 0 \qquad @ \quad y = y_e$

B-5 System Dimensionless Equations with Initial and Boundary Conditions

Matrix: $$\frac{\partial^2 p_{DLm}}{\partial z_D^2} = \frac{3\omega_m}{\lambda_{Ac,fm}} \frac{\partial p_{DLm}}{\partial t_{DAc}} \qquad \text{.....(B-11)}$$

Micro-fractures: $$\frac{\partial^2 p_{DLf}}{\partial x_D^2} = \frac{3\omega_f}{\lambda_{Ac,Ff}} \frac{\partial p_{DLf}}{\partial t_{DAc}} + \frac{\lambda_{Ac,fm}}{\lambda_{Ac,Ff}} \frac{\partial p_{DLm}}{\partial z_D}\Big|_{z_D=1} \qquad \text{.....(B-12)}$$

Macro-fractures: $$\frac{\partial^2 p_{DLF}}{\partial y_D^2} = \omega_F \frac{\partial p_{DLF}}{\partial t_{DAc}} + \frac{\lambda_{Ac,Ff}}{3} \frac{\partial p_{DLf}}{\partial x_D}\Big|_{x_D=1} \qquad \text{.....(B-13)}$$

Dimensionless initial and boundary conditions are:

Matrix:

Initial condition: $p_{DLm}(z_D,0)=0$

Inner boundary: $\dfrac{\partial p_{DLm}}{\partial z_D}=0 \qquad @ \ z_D=0$

Outer boundary: $p_{DLm}=p_{DLf} \qquad @ \ z_D=1$

Micro-fractures:

Initial condition: $p_{DLf}(x_D,0)=0$

Inner boundary: $\dfrac{\partial p_{DLf}}{\partial x_D}=0 \qquad @ \ x_D=0$

Outer boundary: $p_{DLf}=p_{DLF} \qquad @ \ x_D=1$

Macro-fractures:

Initial condition: $p_{DLF}(y_D,0)=0$

Inner boundary: $\left.\dfrac{\partial p_{DLF}}{\partial y_D}\right|_{y_D=0}=-2\pi$

Outer boundary: $\dfrac{\partial p_{DLF}}{\partial y_D}=0 \qquad @ \ y_D=y_{De}={}^{y_e}\!\Big/\!\sqrt{A_{cw}}$

B-6 Laplace Transformation

In order to solve the above system of differential equations, they have to be transformed into Laplace domain for easier solving as detailed below.

Matrix equation:

$$\mathcal{L}\left\{\frac{\partial^2 p_{DLm}}{\partial z_D^2}\right\}=\mathcal{L}\left\{\frac{3\omega_m}{\lambda_{Ac,fm}}\frac{\partial p_{DLm}}{\partial t_{DAc}}\right\} \quad \text{.....(B-14)}$$

$$\frac{\partial^2 \overline{p_{DLm}}}{\partial z_D^2}=\frac{3\omega_m}{\lambda_{Ac,fm}}\left[s\,\overline{p_{DLm}}-\overline{p_{DLm}}(z_D,0)\right] \quad \text{.....(B-15)}$$

The initial and boundary conditions in Laplace domain are:

Initial condition: $\overline{p_{DLm}}(z_D,0)=0$

Inner boundary: $\frac{\partial \overline{p_{DLm}}}{\partial z_D}=0 \qquad @ \ z_D=0$

Outer boundary: $\overline{p_{DLm}}=\overline{p_{DLf}} \qquad @ \ z_D=1$

Using the initial condition, Eq. B-15 becomes

$$\frac{\partial^2 \overline{p_{DLm}}}{\partial z_D^2}=\frac{3\omega_m}{\lambda_{Ac,fm}}\left[s\,\overline{p_{DLm}}-0\right] \qquad \text{(B-16)}$$

$$\frac{\partial^2 \overline{p_{DLm}}}{\partial z_D^2}-\frac{3\omega_m}{\lambda_{Ac,fm}}s\,\overline{p_{DLm}}=0 \qquad \text{(B-17)}$$

The general solution for Eq. B-17 is given by

$$\overline{p_{DLm}}=A\cosh\left(\sqrt{\frac{3s\,\omega_m}{\lambda_{Ac,fm}}}\,z_D\right)+B\sinh\left(\sqrt{\frac{3s\,\omega_m}{\lambda_{Ac,fm}}}\,z_D\right) \qquad \text{(B-18)}$$

The constants A and B are determined as:

1. $z_D=0$:

$$\mathrm{B}=0 \qquad \text{(B-19)}$$

2. $z_D=1$:

$$A=\frac{\overline{p_{DLf}}}{\cosh\left(\sqrt{\frac{3s\,\omega_m}{\lambda_{Ac,fm}}}\right)} \qquad \text{(B-20)}$$

Therefore, the final solution for Eq. B-17 is

$$\overline{p_{DLm}} = \frac{\overline{p_{DLf}}}{\cosh\left(\sqrt{\frac{3s\,\omega_m}{\lambda_{Ac,fm}}}\right)} \cosh\left(\sqrt{\frac{3s\,\omega_m}{\lambda_{Ac,fm}}}\, z_D\right) \quad \text{.....(B-21)}$$

Micro-fractures equation:

$$\mathcal{L}\left\{\frac{\partial^2 p_{DLf}}{\partial x_D^2}\right\} = \mathcal{L}\left\{\frac{3\omega_f}{\lambda_{Ac,Ff}}\frac{\partial p_{DLf}}{\partial t_{DAc}} + \frac{\lambda_{Ac,fm}}{\lambda_{Ac,Ff}}\frac{\partial p_{DLm}}{\partial z_D}\bigg|_{z_D=1}\right\} \quad \text{.....(B-22)}$$

$$\frac{\partial^2 \overline{p_{DLf}}}{\partial x_D^2} = \frac{3\omega_f}{\lambda_{Ac,Ff}}\left[s\,\overline{p_{DLf}} - \overline{p_{DLf}}(x_D,0)\right] + \frac{\lambda_{Ac,fm}}{\lambda_{Ac,Ff}}\frac{\partial \overline{p_{DLm}}}{\partial z_D}\bigg|_{z_D=1} \quad \text{.....(B-23)}$$

The initial and boundary conditions in Laplace domain are:

Initial condition: $\overline{p_{DLf}}(x_D,0) = 0$

Inner boundary: $\dfrac{\partial \overline{p_{DLf}}}{\partial x_D} = 0 \qquad @\ x_D = 0$

Outer boundary: $\overline{p_{DLf}} = \overline{p_{DLF}} \qquad @\ x_D = 1$

Using the initial condition, Eq. B-23 becomes

$$\frac{\partial^2 \overline{p_{DLf}}}{\partial x_D^2} = \frac{3\omega_f}{\lambda_{Ac,Ff}}\,s\,\overline{p_{DLf}} + \frac{\lambda_{Ac,fm}}{\lambda_{Ac,Ff}}\frac{\partial \overline{p_{DLm}}}{\partial z_D}\bigg|_{z_D=1} \quad \text{.....(B-24)}$$

Now, differentiating Eq. B-21, we have

$$\frac{\partial \overline{p_{DLm}}}{\partial z_D}\bigg|_{z_D=1} = \overline{p_{DLf}}\sqrt{\frac{3s\,\omega_m}{\lambda_{Ac,fm}}}\tanh\left(\sqrt{\frac{3s\,\omega_m}{\lambda_{Ac,fm}}}\right) \quad \text{.....(B-25)}$$

Substituting Eq. B-25 in B-24

$$\frac{\partial^2 \overline{p_{DLf}}}{\partial x_D^2} = s\,\overline{p_{DLf}}\left[\frac{3\omega_f}{\lambda_{Ac,Ff}} + \frac{\lambda_{Ac,fm}}{s\,\lambda_{Ac,Ff}}\sqrt{\frac{3s\,\omega_m}{\lambda_{Ac,fm}}}\tanh\left(\sqrt{\frac{3s\,\omega_m}{\lambda_{Ac,fm}}}\right)\right] \quad \text{.....(B-26)}$$

Or in short form

$$\frac{\partial^2 \overline{p_{DLf}}}{\partial x_D^2} - s\,f_f(s)\overline{p_{DLf}} = 0 \quad \text{.....(B-27)}$$

where $f_f(s)$ is

$$f_f(s) = \frac{3\omega_f}{\lambda_{Ac,Ff}} + \frac{\lambda_{Ac,fm}}{s\,\lambda_{Ac,Ff}}\sqrt{\frac{3s\,\omega_m}{\lambda_{Ac,fm}}}\tanh\left(\sqrt{\frac{3s\,\omega_m}{\lambda_{Ac,fm}}}\right) \quad \text{.....(B-28)}$$

The general solution for Eq. B-28 is given by

$$\overline{p_{DLf}} = A\cosh\left(\sqrt{s\,f_f(s)}\,x_D\right) + B\sinh\left(\sqrt{s\,f_f(s)}\,x_D\right) \quad \text{.....(B-29)}$$

The constants A and B are determined as:

1. $x_D = 0$:

$$B = 0 \quad \text{.....(B-30)}$$

2. $x_D = 1$:

$$A = \frac{\overline{p_{DLF}}}{\cosh\left(\sqrt{s\,f_f(s)}\right)} \quad \text{.....(B-31)}$$

Therefore, the final solution for Eq. B-28 is

$$\overline{p_{DLf}} = \frac{\overline{p_{DLF}}}{\cosh\left(\sqrt{s\,f_f(s)}\right)}\cosh\left(\sqrt{s\,f_f(s)}\,x_D\right) \quad \text{.....(B-32)}$$

Macro-fractures equation:

$$\mathcal{L}\left\{\frac{\partial^2 p_{DLF}}{\partial y_D^2}\right\} = \mathcal{L}\left\{\omega_F \frac{\partial p_{DLF}}{\partial t_{DAc}} + \frac{\lambda_{Ac,Ff}}{3}\left.\frac{\partial p_{DLf}}{\partial x_D}\right|_{x_D=1}\right\} \quad \text{(B-33)}$$

$$\frac{\partial^2 \overline{p_{DLF}}}{\partial y_D^2} = \omega_F\left[s\,\overline{p_{DLF}} - \overline{p_{DLF}}(y_D,0)\right] + \frac{\lambda_{Ac,Ff}}{3}\left.\frac{\partial \overline{p_{DLf}}}{\partial x_D}\right|_{x_D=1} \quad \text{(B-34)}$$

The initial and boundary conditions in Laplace domain are:

Initial condition: $\overline{p_{DLF}}(y_D,0) = 0$

Inner boundary: $\left.\frac{\partial \overline{p_{DLF}}}{\partial y_D}\right|_{y_D=0} = -\frac{2\pi}{s}$

Outer boundary: $\frac{\partial \overline{p_{DLF}}}{\partial y_D} = 0 \quad @ \quad y_D = y_{De} = {}^{y_e}\!/\!_{\sqrt{A_{cw}}}$

Using the initial condition, Eq. B-34 becomes

$$\frac{\partial^2 \overline{p_{DLF}}}{\partial y_D^2} = \omega_F\, s\,\overline{p_{DLF}} + \frac{\lambda_{Ac,Ff}}{3}\left.\frac{\partial \overline{p_{DLf}}}{\partial x_D}\right|_{x_D=1} \quad \text{(B-35)}$$

Now differentiating Eq. B-32,

$$\left.\frac{\partial \overline{p_{DLf}}}{\partial x_D}\right|_{x_D=1} = \overline{p_{DLF}}\sqrt{s\,f_f(s)}\,\tanh\left(\sqrt{s\,f_f(s)}\right) \quad \text{(B-36)}$$

Now Eq.B-35 becomes

$$\frac{\partial^2 \overline{p_{DLF}}}{\partial y_D^2} - s\,\overline{p_{DLF}}\left[\omega_F + \frac{\lambda_{Ac,Ff}}{3s}\sqrt{s\,f_f(s)}\,\tanh\left(\sqrt{s\,f_f(s)}\right)\right] = 0 \quad \text{.....(B-37)}$$

Or in short form

$$\frac{\partial^2 \overline{p_{DLF}}}{\partial y_D^2} - s\,f(s)\,\overline{p_{DLF}} = 0 \quad \text{.....(B-38)}$$

where $f(s)$ is definition for the fracture function for Model 1

$$f(s) = \omega_F + \frac{\lambda_{Ac,Ff}}{3s}\sqrt{s\,f_f(s)}\,\tanh\left(\sqrt{s\,f_f(s)}\right)$$

$$f_f(s) = \frac{3\,\omega_f}{\lambda_{Ac,Ff}} + \frac{\lambda_{Ac,fm}}{s\,\lambda_{Ac,Ff}}\sqrt{\frac{3s\,\omega_m}{\lambda_{Ac,fm}}}\,\tanh\left(\sqrt{\frac{3s\,\omega_m}{\lambda_{Ac,fm}}}\right) \quad \text{.....(B-37)}$$

Using this fracture function in Eqs. A-11 or 13 will give the triple-porosity fully transient response for constant rate or constant pressure cases, respectively.

APPENDIX C

DERIVATION OF LINEAR TRIPLE-POROSITY ANALYTICAL SOLUTION FOR MODEL 2

This solution is similar to the previous one with one exception. The matrix – micro-fractures transfer is under pseudo-steady state condition. The same initial and boundary conditions presented in Appendix B are applicable to this model.

C-1 System of Differential Equations

Matrix: $$\frac{12}{L_f^2}\left(p_m - p_f\right) = -\frac{\left[\varphi V \mu c_t\right]_m}{k_m}\frac{\partial p_m}{\partial t} \quad \text{.....(C-1)}$$

Micro-fractures: $$\frac{\partial^2 p_f}{\partial x^2} = \frac{\left[\varphi V \mu c_t\right]_f}{k_f}\frac{\partial p_f}{\partial t} + \frac{\left[\varphi V \mu c_t\right]_m}{k_f}\frac{\partial p_m}{\partial t} \quad \text{.....(C-2)}$$

Macro-fractures: $$\frac{\partial^2 p_F}{\partial y^2} = \frac{\left[\varphi V \mu c_t\right]_F}{k_F}\frac{\partial p_F}{\partial t} + \frac{1}{L_F/2}\frac{k_f}{k_F}\frac{\partial p_f}{\partial x}\bigg|_{x=L_F/2} \quad \text{.....(C-3)}$$

C-2 System of Equations in Dimensionless Form

Matrix: $$\frac{\partial p_{DLm}}{\partial t_{DAc}} = \frac{\lambda_{Ac,fm}}{\omega_m}\left(p_{DLf} - p_{DLm}\right) \quad \text{.....(C-4)}$$

Micro-fractures: $$\frac{\partial^2 p_{DLf}}{\partial x_D^2} = \frac{3\omega_f}{\lambda_{Ac,Ff}}\frac{\partial p_{DLf}}{\partial t_{DAc}} + \frac{3\omega_m}{\lambda_{Ac,Ff}}\frac{\partial p_{DLm}}{\partial t_{DAc}} \quad \text{.....(C-5)}$$

Macro-fractures: $$\frac{\partial^2 p_{DLF}}{\partial y_D^2} = \omega_F\frac{\partial p_{DLF}}{\partial t_{DAc}} + \frac{\lambda_{Ac,Ff}}{3}\frac{\partial p_{DLf}}{\partial x_D}\bigg|_{x_D=1} \quad \text{.....(C-6)}$$

C-3 Laplace Transformation

Matrix equation:

$$\mathcal{L}\left\{\frac{\partial p_{DLm}}{\partial t_{DAc}}\right\} = \mathcal{L}\left\{\frac{\lambda_{Ac,fm}}{\omega_m}\left(p_{DLf} - p_{DLm}\right)\right\} \quad \text{.....(C-7)}$$

$$s\,\overline{p_{DLm}} - \overline{p_{DLm}}(z_D,0) = \frac{\lambda_{Ac,fm}}{\omega_m}\left(\overline{p_{DLf}} - \overline{p_{DLm}}\right) \quad \text{.....(C-8)}$$

Using the initial condition, Eq. C-8 becomes

$$s\,\overline{p_{DLm}} = \frac{\lambda_{Ac,fm}}{\omega_m}\left(\overline{p_{DLf}} - \overline{p_{DLm}}\right) \quad \text{.....(C-9)}$$

Thus,

$$\overline{p_{DLm}} = \frac{\lambda_{Ac,fm}}{\left[s\omega_m + \lambda_{Ac,fm}\right]}\overline{p_{DLf}} \quad \text{.....(C-10)}$$

Micro-fractures equation:

$$\mathcal{L}\left\{\frac{\partial^2 p_{DLf}}{\partial x_D^2}\right\} = \mathcal{L}\left\{\frac{3\omega_f}{\lambda_{Ac,Ff}}\frac{\partial p_{DLf}}{\partial t_{DAc}} + \frac{3\omega_m}{\lambda_{Ac,Ff}}\frac{\partial p_{DLm}}{\partial t_{DAc}}\right\} \text{.....(C-11)}$$

$$\frac{\partial^2 \overline{p_{DLf}}}{\partial x_D^2} = \frac{3\omega_f}{\lambda_{Ac,Ff}}\left[s\,\overline{p_{DLf}} - \overline{p_{DLf}}(x_D,0)\right] + \frac{3\omega_m}{\lambda_{Ac,Ff}}\left[s\,\overline{p_{DLm}} - \overline{p_{DLm}}(z_D,0)\right] \text{.....(C-12)}$$

Using the initial condition, Eq. C-12 becomes

$$\frac{\partial^2 \overline{p_{DLf}}}{\partial x_D^2} = \frac{3\omega_f s}{\lambda_{Ac,Ff}}\overline{p_{DLf}} + \frac{3s\,\omega_m}{\lambda_{Ac,Ff}}\overline{p_{DLm}} \quad \text{.....(C-13)}$$

Now, substituting Eq. C-10 into Eq. C-13, we have

$$\frac{\partial^2 \overline{p_{DLf}}}{\partial x_D^2} = s\overline{p_{DLf}}\left[\frac{3\omega_f}{\lambda_{Ac,Ff}} + \frac{3\omega_m \lambda_{Ac,fm}}{s\omega_m \lambda_{Ac,Ff} + \lambda_{Ac,fm}\lambda_{Ac,Ff}}\right] \quad \text{(C-14)}$$

Or in short form

$$\frac{\partial^2 \overline{p_{DLf}}}{\partial x_D^2} - s\, f_f(s)\overline{p_{DLf}} = 0 \quad \text{(C-15)}$$

Where $f_f(s)$ is

$$f_f(s) = \frac{3\omega_f}{\lambda_{Ac,Ff}} + \frac{3\omega_m \lambda_{Ac,fm}}{s\omega_m \lambda_{Ac,Ff} + \lambda_{Ac,fm}\lambda_{Ac,Ff}} \quad \text{(C-16)}$$

The general solution for Eq. C-15 is given by

$$\overline{p_{DLf}} = A\cosh\left(\sqrt{s\, f_f(s)}\, x_D\right) + B\sinh\left(\sqrt{s\, f_f(s)}\, x_D\right) \quad \text{(C-17)}$$

The constants A and B are determined as:

1. $x_D = 0$:

$$B = 0 \quad \text{(C-18)}$$

2. $x_D = 1$:

$$A = \frac{\overline{p_{DLF}}}{\cosh\left(\sqrt{s\, f_f(s)}\right)} \quad \text{(C-19)}$$

Therefore, the final solution for Eq. C-15 is

$$\overline{p_{DLf}} = \frac{\overline{p_{DLF}}}{\cosh\left(\sqrt{s\, f_f(s)}\right)}\cosh\left(\sqrt{s\, f_f(s)}\, x_D\right) \quad \text{(C-20)}$$

Macro-fractures equation:

$$\mathcal{L}\left\{\frac{\partial^2 p_{DLF}}{\partial y_D^2}\right\} = \mathcal{L}\left\{\omega_F \frac{\partial p_{DLF}}{\partial t_{DAc}} + \frac{\lambda_{Ac,Ff}}{3}\frac{\partial p_{DLf}}{\partial x_D}\bigg|_{x_D=1}\right\} \quad \text{(C-21)}$$

$$\frac{\partial^2 \overline{p_{DLF}}}{\partial y_D^2} = \omega_F\left[s\,\overline{p_{DLF}} - \overline{p_{DLF}}(y_D,0)\right] + \frac{\lambda_{Ac,Ff}}{3}\frac{\partial \overline{p_{DLf}}}{\partial x_D}\bigg|_{x_D=1} \quad \text{(C-22)}$$

Using the initial condition, Eq. C-22 becomes

$$\frac{\partial^2 \overline{p_{DLF}}}{\partial y_D^2} = \omega_F\, s\,\overline{p_{DLF}} + \frac{\lambda_{Ac,Ff}}{3}\frac{\partial \overline{p_{DLf}}}{\partial x_D}\bigg|_{x_D=1} \quad \text{(C-23)}$$

Now differentiating Eq. C-20,

$$\frac{\partial \overline{p_{DLf}}}{\partial x_D}\bigg|_{x_D=1} = \overline{p_{DLF}}\sqrt{s\,f_f(s)}\,\tanh\left(\sqrt{s\,f_f(s)}\right) \quad \text{(C-24)}$$

Now Eq. C-23 becomes

$$\frac{\partial^2 \overline{p_{DLF}}}{\partial y_D^2} - s\,\overline{p_{DLF}}\left[\omega_F + \frac{\lambda_{Ac,Ff}}{3s}\sqrt{s\,f_f(s)}\,\tanh\left(\sqrt{s\,f_f(s)}\right)\right] = 0 \quad \text{(C-25)}$$

Or in short form

$$\frac{\partial^2 \overline{p_{DLF}}}{\partial y_D^2} - s\,f(s)\,\overline{p_{DLF}} = 0 \quad \text{(C-26)}$$

where $f(s)$ is

$$f(s) = \omega_F + \frac{\lambda_{Ac,Ff}}{3s}\sqrt{s\,f_f(s)}\,\tanh\left(\sqrt{s\,f_f(s)}\right)$$
$$f_f(s) = \frac{3\omega_f}{\lambda_{Ac,Ff}} + \frac{3\omega_m\lambda_{Ac,fm}}{s\omega_m\lambda_{Ac,Ff} + \lambda_{Ac,fm}\lambda_{Ac,Ff}} \quad \text{(C-53)}$$

APPENDIX D

DERIVATION OF LINEAR TRIPLE-POROSITY ANALYTICAL SOLUTION FOR MODEL 3

In this section, the triple-porosity solution is derived for the system with transient interporosity flow between matrix and micro-fractures and pseudo-steady state flow between the two fractures systems.

D-1 System of Differential Equations

Matrix: $$\frac{\partial^2 p_m}{\partial z^2} = \frac{[\varphi V \mu c_t]_m}{k_m} \frac{\partial p_m}{\partial t} \quad \text{.....(D-1)}$$

Micro-fractures: $$-\frac{12}{L_F^2}\left(p_f - p_F\right) = \frac{[\varphi V \mu c_t]_f}{k_f} \frac{\partial p_f}{\partial t} + \frac{1}{L_f/2} \frac{k_m}{k_f} \frac{\partial p_m}{\partial z}\bigg|_{z=L_f/2} \quad \text{.....(D-2)}$$

Macro-fractures: $$\frac{\partial^2 p_F}{\partial y^2} = \frac{[\varphi V \mu c_t]_F}{k_F} \frac{\partial p_F}{\partial t} + \frac{[\varphi V \mu c_t]_f}{k_F} \frac{\partial p_f}{\partial t} + \frac{1}{L_f/2} \frac{k_m}{k_F} \frac{\partial p_m}{\partial z}\bigg|_{z=L_f/2} \quad \text{....(D-3)}$$

D-2 System of Differential Equations in Dimensionless Form

Matrix: $$\frac{\partial^2 p_{DLm}}{\partial z_D^2} = \frac{3\omega_m}{\lambda_{Ac,fm}} \frac{\partial p_{DLm}}{\partial t_{DAc}} \quad \text{.....(D-4)}$$

Micro-fractures: $$\left(p_{DLF} - p_{DLf}\right) = \frac{\omega_f}{\lambda_{Ac,Ff}} \frac{\partial p_{DLf}}{\partial t_{DAc}} + \frac{1}{3} \frac{\lambda_{Ac,fm}}{\lambda_{Ac,Ff}} \frac{\partial p_{DLm}}{\partial z_D}\bigg|_{z_D=1} \quad \text{.....(D-5)}$$

Macro-fractures: $$\frac{\partial^2 p_{DLF}}{\partial y_D^2} = \omega_F \frac{\partial p_{DLF}}{\partial t_{DAc}} + \omega_f \frac{\partial p_{DLf}}{\partial t_{DAc}} + \frac{\lambda_{Ac,fm}}{3} \frac{\partial p_{DLm}}{\partial z_D}\bigg|_{z_D=1} \quad \text{.....(D-6)}$$

D-3 Laplace Transformation

Matrix equation:

$$\mathcal{L}\left\{\frac{\partial^2 p_{DLm}}{\partial z_D^2}\right\} = \mathcal{L}\left\{\frac{3\omega_m}{\lambda_{Ac,fm}}\frac{\partial p_{DLm}}{\partial t_{DAc}}\right\} \quad \text{.....(D-7)}$$

$$\frac{\partial^2 \overline{p_{DLm}}}{\partial z_D^2} = \frac{3\omega_m}{\lambda_{Ac,fm}}\left[s\,\overline{p_{DLm}} - \overline{p_{DLm}}(z_D,0)\right] \quad \text{.....(D-8)}$$

Using the initial condition, Eq. D-8 becomes

$$\frac{\partial^2 \overline{p_{DLm}}}{\partial z_D^2} - \frac{3\omega_m}{\lambda_{Ac,fm}} s\,\overline{p_{DLm}} = 0 \quad \text{.....(D-9)}$$

The general solution for Eq. D-9 is given by

$$\overline{p_{DLm}} = A\cosh\left(\sqrt{\frac{3s\,\omega_m}{\lambda_{Ac,fm}}}\,z_D\right) + B\sinh\left(\sqrt{\frac{3s\,\omega_m}{\lambda_{Ac,fm}}}\,z_D\right) \quad \text{.....(D-10)}$$

The constants A and B are determined as:

1. $z_D = 0$:

$$\text{B} = 0 \quad \text{.....(D-11)}$$

2. $z_D = 1$:

$$A = \frac{\overline{p_{DLf}}}{\cosh\left(\sqrt{\frac{3s\,\omega_m}{\lambda_{Ac,fm}}}\right)} \quad \text{.....(D-12)}$$

Therefore, the final solution for Eq. D-9 is

$$\overline{p_{DLm}} = \frac{\overline{p_{DLf}}}{\cosh\left(\sqrt{\frac{3s\,\omega_m}{\lambda_{Ac,fm}}}\right)}\cosh\left(\sqrt{\frac{3s\,\omega_m}{\lambda_{Ac,fm}}}\,z_D\right) \quad \text{.....(D-13)}$$

Micro-fractures equation:

$$\mathcal{L}\{p_{DLF} - p_{DLf}\} = \mathcal{L}\left\{\frac{\omega_f}{\lambda_{Ac,Ff}}\frac{\partial p_{DLf}}{\partial t_{DAc}} + \frac{1}{3}\frac{\lambda_{Ac,fm}}{\lambda_{Ac,Ff}}\frac{\partial p_{DLm}}{\partial z_D}\bigg|_{z_D=1}\right\} \quad \text{.....(D-14)}$$

$$\overline{p_{DLF}} - \overline{p_{DLf}} = \frac{\omega_f}{\lambda_{Ac,Ff}}\left[s\,\overline{p_{DLf}} - \overline{p_{DLf}}(x_D,0)\right] + \frac{1}{3}\frac{\lambda_{Ac,fm}}{\lambda_{Ac,Ff}}\frac{\partial \overline{p_{DLm}}}{\partial z_D}\bigg|_{z_D=1} \quad \text{.....(D-15)}$$

Using the initial condition, Eq. D-15 becomes

$$\overline{p_{DLF}} - \overline{p_{DLf}} = \frac{\omega_f}{\lambda_{Ac,Ff}}\,s\,\overline{p_{DLf}} + \frac{1}{3}\frac{\lambda_{Ac,fm}}{\lambda_{Ac,Ff}}\frac{\partial \overline{p_{DLm}}}{\partial z_D}\bigg|_{z_D=1} \quad \text{.....(D-16)}$$

Now, differentiating Eq. D-13, we have

$$\frac{\partial \overline{p_{DLm}}}{\partial z_D}\bigg|_{z_D=1} = \overline{p_{DLf}}\sqrt{\frac{3s\,\omega_m}{\lambda_{Ac,fm}}}\tanh\left(\sqrt{\frac{3s\,\omega_m}{\lambda_{Ac,fm}}}\right) \quad \text{.....(D-17)}$$

Substituting Eq. D-17 in D-16

$$\overline{p_{DLF}} - \overline{p_{DLf}} = \frac{\omega_f}{\lambda_{Ac,Ff}}\,s\,\overline{p_{DLf}} + \frac{1}{3}\frac{\lambda_{Ac,fm}}{\lambda_{Ac,Ff}}\,\overline{p_{DLf}}\sqrt{\frac{3s\,\omega_m}{\lambda_{Ac,fm}}}\tanh\left(\sqrt{\frac{3s\,\omega_m}{\lambda_{Ac,fm}}}\right) \quad \text{.....(D-18)}$$

$$\overline{p_{DLf}} = \overline{p_{DLF}}\left[\frac{3\lambda_{Ac,Ff}}{3\lambda_{Ac,Ff} + 3s\omega_f + \lambda_{Ac,fm}\sqrt{\frac{3s\,\omega_m}{\lambda_{Ac,fm}}}\tanh\left(\sqrt{\frac{3s\,\omega_m}{\lambda_{Ac,fm}}}\right)}\right] \quad \text{.....(D-19)}$$

Macro-fractures equation:

$$\mathcal{L}\left\{\frac{\partial^2 p_{DLF}}{\partial y_D^2}\right\}=\mathcal{L}\left\{\omega_F\frac{\partial p_{DLF}}{\partial t_{DAc}}+\omega_f\frac{\partial p_{DLf}}{\partial t_{DAc}}+\frac{\lambda_{Ac,fm}}{3}\frac{\partial p_{DLm}}{\partial z_D}\bigg|_{z_D=1}\right\} \quad \text{.....(D-20)}$$

$$\frac{\partial^2 \overline{p_{DLF}}}{\partial y_D^2}=\omega_F\left[s\,\overline{p_{DLF}}-\overline{p_{DLF}}(y_D,0)\right]+\omega_f\left[s\,\overline{p_{DLf}}-\overline{p_{DLf}}(x_D,0)\right]+\frac{\lambda_{Ac,fm}}{3}\frac{\partial \overline{p_{DLm}}}{\partial z_D}\bigg|_{z_D=1} \quad \text{.....}$$

$$\text{.....(D-21)}$$

Using the initial condition, Eq. D-21 becomes

$$\frac{\partial^2 \overline{p_{DLF}}}{\partial y_D^2}=\omega_F s\,\overline{p_{DLF}}+\omega_f s\,\overline{p_{DLf}}+\frac{\lambda_{Ac,fm}}{3}\frac{\partial \overline{p_{DLm}}}{\partial z_D}\bigg|_{z_D=1} \quad \text{.....(D-22)}$$

After substituting Eq. D-17 and D-19 in D-22 and after algebraic manipulation, we have

$$\frac{\partial^2 \overline{p_{DLF}}}{\partial y_D^2}=s\,\overline{p_{DLF}}\left[\omega_F+\frac{3\omega_f\lambda_{Ac,Ff}+\frac{\lambda_{Ac,Ff}\lambda_{Ac,fm}}{s}\sqrt{\frac{3s\,\omega_m}{\lambda_{Ac,fm}}}\tanh\left(\sqrt{\frac{3s\,\omega_m}{\lambda_{Ac,fm}}}\right)}{3\lambda_{Ac,Ff}+3s\omega_f+\lambda_{Ac,fm}\sqrt{\frac{3s\,\omega_m}{\lambda_{Ac,fm}}}\tanh\left(\sqrt{\frac{3s\,\omega_m}{\lambda_{Ac,fm}}}\right)}\right] \quad \text{.....(D-23)}$$

Or in short form

$$\frac{\partial^2 \overline{p_{DLF}}}{\partial y_D^2}-s\,f(s)\,\overline{p_{DLF}}=0 \quad \text{.....(D-24)}$$

where $f(s)$ is

$$f(s)=\omega_F+\frac{3\omega_f\lambda_{Ac,Ff}+\frac{\lambda_{Ac,Ff}\lambda_{Ac,fm}}{s}\sqrt{\frac{3s\,\omega_m}{\lambda_{Ac,fm}}}\tanh\left(\sqrt{\frac{3s\,\omega_m}{\lambda_{Ac,fm}}}\right)}{3\lambda_{Ac,Ff}+3s\omega_f+\lambda_{Ac,fm}\sqrt{\frac{3s\,\omega_m}{\lambda_{Ac,fm}}}\tanh\left(\sqrt{\frac{3s\,\omega_m}{\lambda_{Ac,fm}}}\right)} \quad \text{.....(D-25)}$$

APPENDIX E

DERIVATION OF LINEAR TRIPLE-POROSITY ANALYTICAL SOLUTION FOR FULLY PSEUDOSTEADY STATE FLUID TRANSFER– MODEL 4

In this section, the triple-porosity solution is derived for a system with pseudosteady state interporosity flow between matrix and micro-fractures the two fractures systems.

E-1 System of Differential Equations

Matrix: $$\frac{12}{L_f^2}\left(p_m - p_f\right) = -\frac{\left[\varphi V \mu c_t\right]_m}{k_m}\frac{\partial p_m}{\partial t} \quad \text{..... (E-1)}$$

Micro-fractures: $$-\frac{12}{L_f^2}\left(p_f - p_F\right) = \frac{\left[\varphi V \mu c_t\right]_m}{k_f}\frac{\partial p_m}{\partial t} + \frac{\left[\varphi V \mu c_t\right]_f}{k_f}\frac{\partial p_f}{\partial t} \quad \text{..... (E-2)}$$

Macro-fractures: $$\frac{\partial^2 p_F}{\partial y^2} = \frac{\left[\varphi V \mu c_t\right]_m}{k_F}\frac{\partial p_m}{\partial t} + \frac{\left[\varphi V \mu c_t\right]_f}{k_F}\frac{\partial p_f}{\partial t} + \frac{\left[\varphi V \mu c_t\right]_F}{k_F}\frac{\partial p_F}{\partial t} \quad \text{..... (E-3)}$$

E-2 System of Differential Equations in Dimensionless Form

Matrix: $$\frac{\partial p_{DLm}}{\partial t_{DAc}} = \frac{\lambda_{Ac,fm}}{\omega_m}\left(p_{DLf} - p_{DLm}\right) \quad \text{..... (E-4)}$$

Micro-fractures: $$\frac{\partial p_{DLf}}{\partial t_{DAc}} = \frac{\lambda_{Ac,Ff}}{\omega_f}\left(p_{DLF} - p_{DLf}\right) - \frac{\omega_m}{\omega_f}\frac{\partial p_{DLm}}{\partial t_{DAc}} \quad \text{..... (E-5)}$$

Macro-fractures: $$\frac{\partial^2 p_{DLF}}{\partial y_D^2} = \omega_m \frac{\partial p_{DLm}}{\partial t_{DAc}} + \omega_f \frac{\partial p_{DLf}}{\partial t_{DAc}} + \omega_F \frac{\partial p_{DLF}}{\partial t_{DAc}} \quad \text{..... (E-6)}$$

E-3 Laplace Transformation

Matrix equation:

$$\mathcal{L}\left\{\frac{\partial p_{DLm}}{\partial t_{DAc}}\right\} = \mathcal{L}\left\{\frac{\lambda_{Ac,fm}}{\omega_m}\left(p_{DLf} - p_{DLm}\right)\right\} \quad \text{..... (E-7)}$$

$$s\,\overline{p_{DLm}} - \overline{p_{DLm}}(z_D,0) = \frac{\lambda_{Ac,fm}}{\omega_m}\left(\overline{p_{DLf}} - \overline{p_{DLm}}\right) \quad \text{..... (E-8)}$$

Using the initial condition, Eq. E-8 becomes

$$s\,\overline{p_{DLm}} = \frac{\lambda_{Ac,fm}}{\omega_m}\left(\overline{p_{DLf}} - \overline{p_{DLm}}\right) \quad \text{..... (E-9)}$$

Thus,

$$\overline{p_{DLm}} = \frac{\lambda_{Ac,fm}}{\left[s\,\omega_m + \lambda_{Ac,fm}\right]}\overline{p_{DLf}} \quad \text{..... (E-10)}$$

Micro-fractures equation:

$$\mathcal{L}\left\{\frac{\partial p_{DLf}}{\partial t_{DAc}}\right\} = \mathcal{L}\left\{\frac{\lambda_{Ac,Ff}}{\omega_f}\left(p_{DLF} - p_{DLf}\right) - \frac{\omega_m}{\omega_f}\frac{\partial p_{DLm}}{\partial t_{DAc}}\right\} \text{..... (E-11)}$$

$$s\,\overline{p_{DLf}} - \overline{p_{DLf}}(x_D,0) = \frac{\lambda_{Ac,Ff}}{\omega_f}\left(\overline{p_{DLF}} - \overline{p_{DLf}}\right) - \frac{\omega_m}{\omega_f}\left[s\,\overline{p_{DLm}} - \overline{p_{DLm}}(z_D,0)\right] \text{..... (E-12)}$$

Using the initial condition, Eq. E-12 becomes

$$s\,\overline{p_{DLf}} = \frac{\lambda_{Ac,Ff}}{\omega_f}\left(\overline{p_{DLF}} - \overline{p_{DLf}}\right) - \frac{\omega_m}{\omega_f}s\,\overline{p_{DLm}} \text{..... (E-13)}$$

Substituting Eq. E-10 in E-13 and after algebraic manipulation, we have

$$s\overline{p_{DLf}} = \frac{\lambda_{Ac,Ff}}{\omega_f}\left(\overline{p_{DLF}} - \overline{p_{DLf}}\right) - \frac{\omega_m}{\omega_f} s \frac{\lambda_{Ac,fm}}{\left[s\omega_m + \lambda_{Ac,fm}\right]}\overline{p_{DLf}} \quad \text{..... (E-14)}$$

$$\overline{p_{DLf}} = \left(\frac{\lambda_{Ac,Ff}\left(s\omega_m + \lambda_{Ac,fm}\right)}{\left(\lambda_{Ac,Ff} + s\omega_f\right)\left(s\omega_m + \lambda_{Ac,fm}\right) + s\omega_m\lambda_{Ac,fm}} \right)\overline{p_{DLF}} \quad \text{..... (E-15)}$$

Macro-fractures equation:

$$\mathcal{L}\left\{\frac{\partial^2 p_{DLF}}{\partial y_D^2}\right\} = \mathcal{L}\left\{\omega_m \frac{\partial p_{DLm}}{\partial t_{DAc}} + \omega_f \frac{\partial p_{DLf}}{\partial t_{DAc}} + \omega_F \frac{\partial p_{DLF}}{\partial t_{DAc}}\right\} \quad \text{..... (E-16)}$$

$$\frac{\partial^2 \overline{p_{DLF}}}{\partial y_D^2} = \omega_m\left[s\overline{p_{DLm}} - \overline{p_{DLm}}(z_D,0)\right] + \omega_f\left[s\overline{p_{DLf}} - \overline{p_{DLf}}(x_D,0)\right] + \omega_F\left[s\overline{p_{DLF}} - \overline{p_{DLF}}(y_D,0)\right]$$
..... (E-17)

Using the initial condition, Eq. E-17 becomes

$$\frac{\partial^2 \overline{p_{DLF}}}{\partial y_D^2} = \omega_m\left[s\overline{p_{DLm}}\right] + \omega_f\left[s\overline{p_{DLf}}\right] + \omega_F\left[s\overline{p_{DLF}}\right] \quad \text{..... (E-18)}$$

Now substituting Eq. E-10 and E-15 in E-18,

$$\frac{\partial^2 \overline{p_{DLF}}}{\partial y_D^2} = \omega_m \frac{\lambda_{Ac,fm}}{\left[s\left(1-\omega_f-\omega_F\right) + \lambda_{Ac,fm}\right]} s\overline{p_{DLf}} + \frac{\omega_f \lambda_{Ac,Ff}\left(s\omega_m + \lambda_{Ac,fm}\right)}{\left(\lambda_{Ac,Ff} + s\omega_f\right)\left(s\omega_m + \lambda_{Ac,fm}\right) + s\omega_m\lambda_{Ac,fm}} s\overline{p_{DLF}} + \omega_F s\overline{p_{DLF}} \quad \text{..... (E-19)}$$

$$\frac{\partial^2 \overline{p_{DLF}}}{\partial y_D^2} = s\overline{p_{DLF}}\left[\omega_F + \frac{\omega_m\lambda_{Ac,fm}\lambda_{Ac,Ff} + \omega_f\lambda_{Ac,Ff}\left(s\omega_m + \lambda_{Ac,fm}\right)}{\left(\lambda_{Ac,Ff} + s\omega_f\right)\left(s\omega_m + \lambda_{Ac,fm}\right) + s\omega_m\lambda_{Ac,fm}}\right] \quad \text{..... (E-20)}$$

$$\frac{\partial^2 \overline{p_{DLF}}}{\partial y_D^2} = s\overline{p_{DLF}}\left[\omega_F + \frac{\lambda_{Ac,Ff}\left[\omega_m\lambda_{Ac,fm} + \omega_f\left(s\omega_m + \lambda_{Ac,fm}\right)\right]}{\left(\lambda_{Ac,Ff} + s\omega_f\right)\left(s\omega_m + \lambda_{Ac,fm}\right) + s\omega_m\lambda_{Ac,fm}}\right] \quad \text{..... (E-21)}$$

Or in short form

$$\frac{\partial^2 \overline{p_{DLF}}}{\partial y_D^2} - s f(s) \overline{p_{DLF}} = 0 \quad \text{..... (E-22)}$$

where $f(s)$ is

$$f(s) = \omega_F + \frac{\lambda_{Ac,Ff}\left[\omega_m \lambda_{Ac,fm} + \omega_f \left(s\omega_m + \lambda_{Ac,fm}\right)\right]}{\left(\lambda_{Ac,Ff} + s\omega_f\right)\left(s\omega_m + \lambda_{Ac,fm}\right) + s\omega_m \lambda_{Ac,fm}} \quad \text{..... (E-23)}$$

APPENDIX F

EFFECTS OF TRIPLE-POROSITY PARAMETERS ON MODEL 1 RESPONSE

This appendix presents a series of figures showing the effect of triple-porosity parameters on Model 1 response for constant pressure case. These parameters are ω_F, ω_f, $\lambda_{Ac,fm}$, $\lambda_{Ac,Ff}$ and y_{eD}.

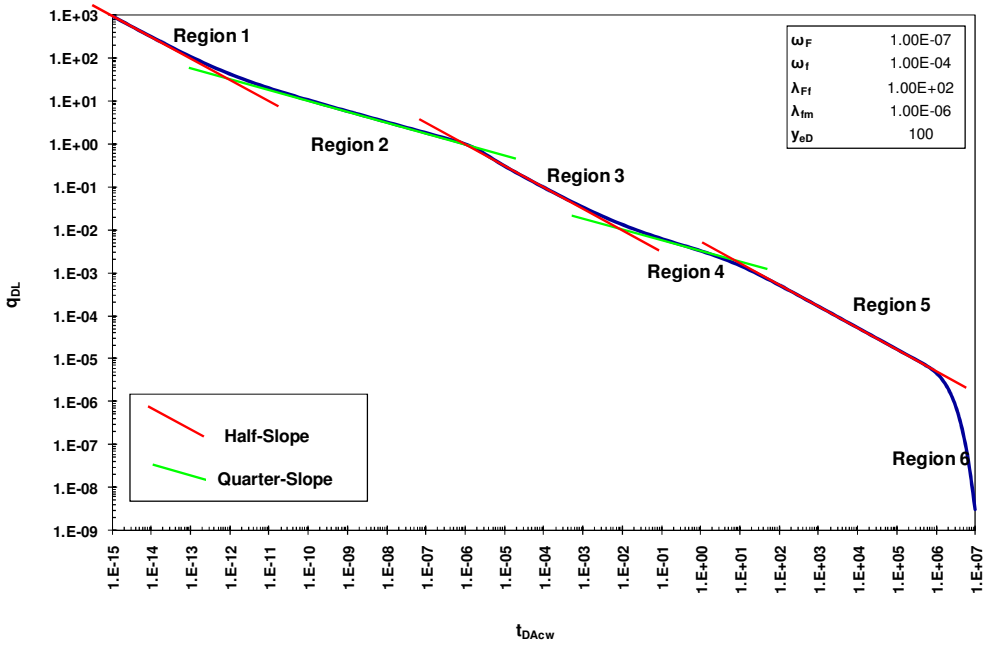

Fig. F-1 – Model 1 constant pressure solution: base case.

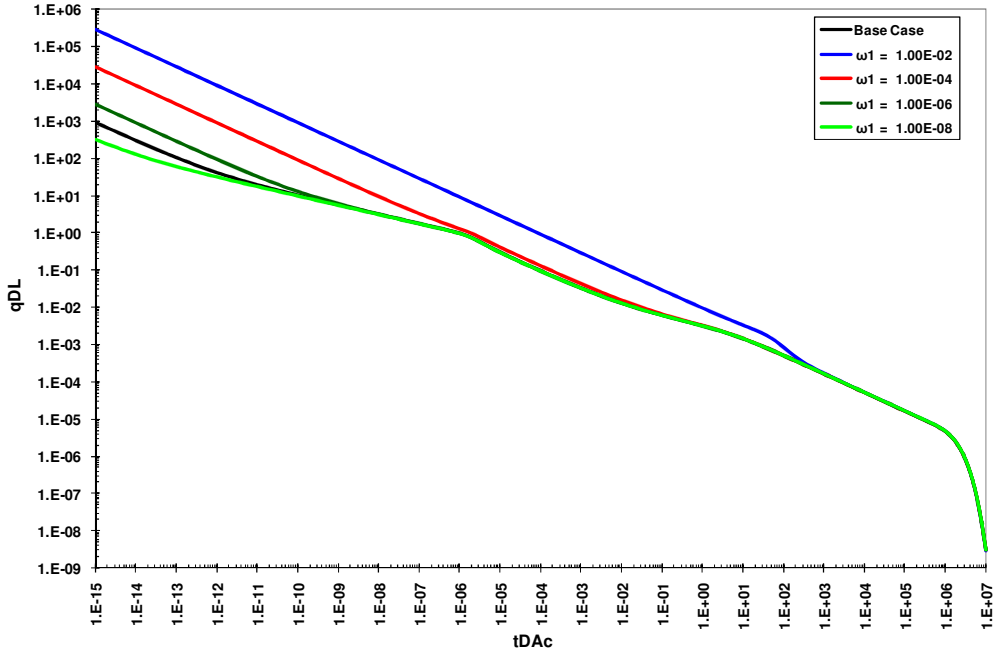

Fig. F-2 – Effect of ω_F on Model 1 constant pressure solution.

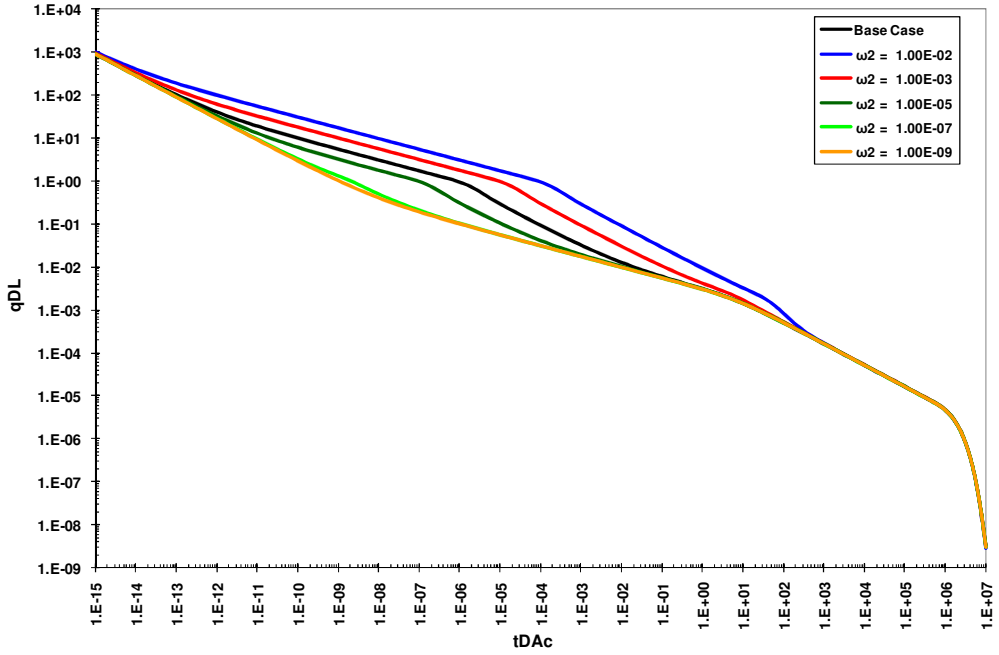

Fig. F-3 – Effect of ω_f on Model 1 constant pressure solution.

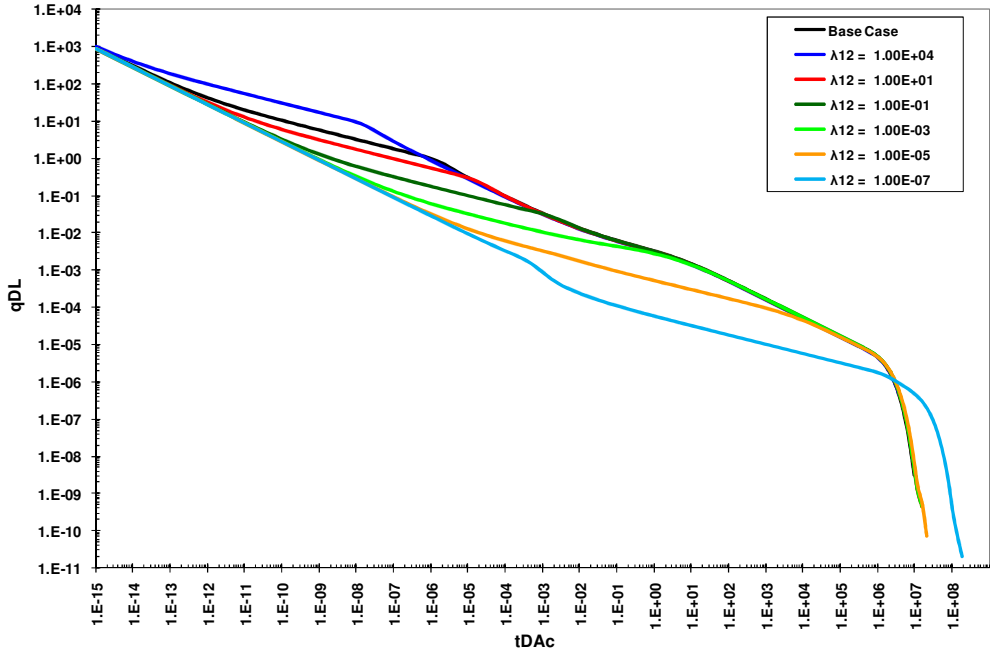

Fig. F-4 – Effect of $\lambda_{Ac,Ff}$ on Model 1 constant pressure solution.

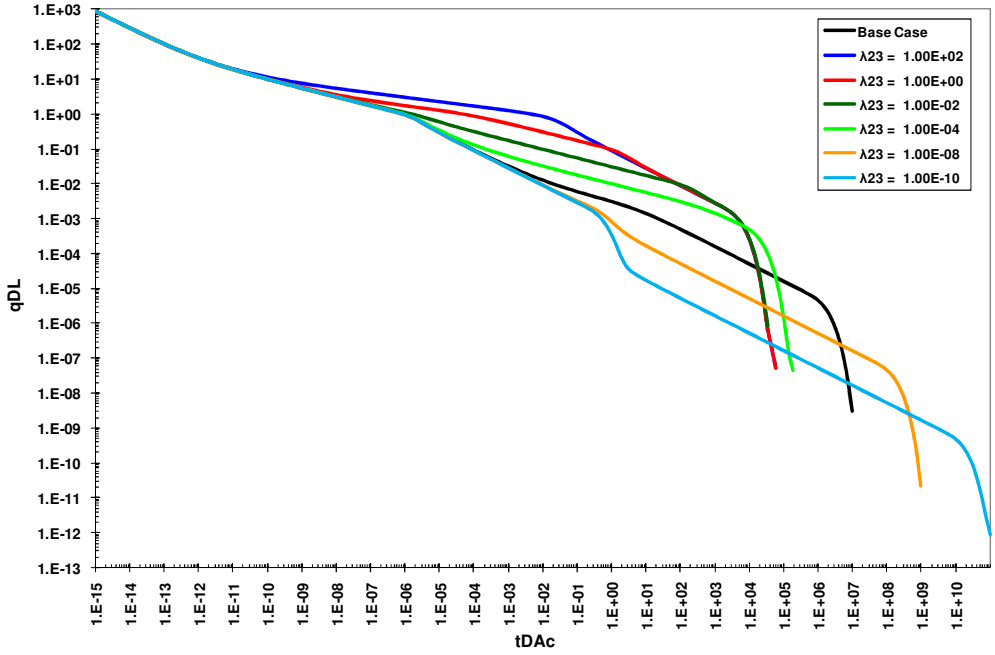

Fig. F-5 – Effect of $\lambda_{Ac,fm}$ on Model 1 constant pressure solution.

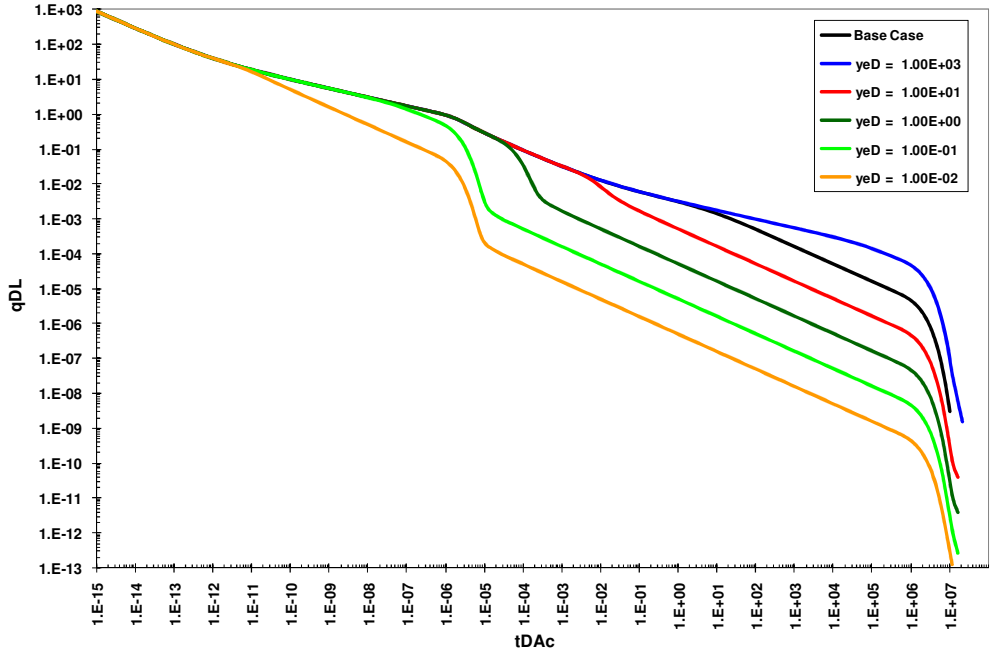

Fig. F-6 – Effect of y_{eD} on Model 1 constant pressure solution.

APPENDIX G

SUMMARY OF SOLUTIONS

This appendix provides a summary of the triple-porosity solutions derived in this work in addition to definitions of dimensionless variables.

G-1 Dimensionless Variables Definitions

Table G-1 – Dimensionless variables for triple-porosity radial reservoirs

Fluid	Constant Rate	Constant Pressure
Oil	$p_D = \frac{k_F h(p_i - p)}{141.2\,qB\mu}$	$\frac{1}{q_D} = \frac{k_F h(p_i - p)}{141.2\,qB\mu}$
	$t_D = \frac{0.00633 k_F t}{\mu[\varphi V c_t]_t r_w^2}$	
Gas	$m_D = \frac{k_F h[m(p_i) - m(p)]}{1422\,q_g T}$	$\frac{1}{q_D} = \frac{k_F h[m(p_i) - m(p)]}{1422\,q_g T}$
	$t_D = \frac{0.00633 k_F t}{\mu[\varphi V c_t]_{ti} r_w^2}$	
Both	$r_D = \frac{r}{r_w}$	

Table G-2 – Dimensionless variables for triple-porosity linear reservoirs		
Fluid	Constant Rate	Constant Pressure
Oil	$p_{DL} = \frac{k_F \sqrt{A_{cw}}(p_i - p)}{141.2\, qB\mu}$	$\frac{1}{q_{DL}} = \frac{k_F \sqrt{A_{cw}}(p_i - p)}{141.2\, qB\mu}$
	$t_{DAc} = \frac{0.00633 k_F t}{\mu[\varphi V c_t]_t A_{cw}}$	
Gas	$m_{DL} = \frac{k_F \sqrt{A_{cw}}\,[m(p_i) - m(p)]}{1422\, q_g T}$	$\frac{1}{q_{DL}} = \frac{k_F \sqrt{A_{cw}}\,[m(p_i) - m(p)]}{1422\, q_g T}$
	$t_{DAc} = \frac{0.00633 k_F t}{\mu[\varphi V c_t]_{ti} A_{cw}}$	
Both	$y_D = \frac{y}{\sqrt{A_{cw}}}$	

G-2 Radial and Linear Flow Solutions at the Well

Table G-3 – Radial flow solutions for closed reservoir	
Constant Rate	$\overline{p_{wD}} = \frac{\left[I_0\left(\sqrt{s\,f(s)}\right)K_1\left(\sqrt{s\,f(s)}\,r_{eD}\right) + I_1\left(\sqrt{s\,f(s)}\,r_{eD}\right)K_0\left(\sqrt{s\,f(s)}\right)\right]}{s\sqrt{s\,f(s)}\left[I_1\left(\sqrt{s\,f(s)}\,r_{eD}\right)K_1\left(\sqrt{s\,f(s)}\right) + I_1\left(\sqrt{s\,f(s)}\right)K_1\left(\sqrt{s\,f(s)}\,r_{eD}\right)\right]}$
Constant Pressure	$\frac{1}{\overline{q_D}} = \frac{s\left[I_0\left(\sqrt{s\,f(s)}\right)K_1\left(\sqrt{s\,f(s)}\,r_{eD}\right) + I_1\left(\sqrt{s\,f(s)}\,r_{eD}\right)K_0\left(\sqrt{s\,f(s)}\right)\right]}{\sqrt{s\,f(s)}\left[I_1\left(\sqrt{s\,f(s)}\,r_{eD}\right)K_1\left(\sqrt{s\,f(s)}\right) + I_1\left(\sqrt{s\,f(s)}\right)K_1\left(\sqrt{s\,f(s)}\,r_{eD}\right)\right]}$

Table G-4 – Linear flow solutions for closed reservoir	
Constant Rate	$\overline{p_{wDL}} = \frac{2\pi}{s\sqrt{s\,f(s)}}\left[\frac{1+\exp\left(-2\sqrt{s\,f(s)}y_{De}\right)}{1-\exp\left(-2\sqrt{s\,f(s)}y_{De}\right)}\right]$
Constant Pressure	$\frac{1}{\overline{q_{DL}}} = \frac{2\pi s}{\sqrt{s\,f(s)}}\left[\frac{1+\exp\left(-2\sqrt{s\,f(s)}y_{De}\right)}{1-\exp\left(-2\sqrt{s\,f(s)}y_{De}\right)}\right]$

For complete list of solutions, refer to El-Banbi Dissertation (El-Banbi 1998).

G-3 Fracture Functions for Triple-porosity System

Table G-5 – Fracture functions derived for triple-porosity model	
Model	Fracture Function, $f(s)$
Triple-Porosity Fully Transient (Model 1)	$f(s) = \omega_F + \frac{\lambda_{Ac,Ff}}{3s}\sqrt{s\,f_f(s)}\,\tanh\left(\sqrt{s\,f_f(s)}\right)$ $f_f(s) = \frac{3\omega_f}{\lambda_{Ac,Ff}} + \frac{\lambda_{Ac,fm}}{s\lambda_{Ac,Ff}}\sqrt{\frac{3s\omega_m}{\lambda_{Ac,fm}}}\tanh\left(\sqrt{\frac{3s\omega_m}{\lambda_{Ac,fm}}}\right)$
Triple-Porosity Mixed Flow (Model 2)	$f(s) = \omega_F + \frac{\lambda_{Ac,Ff}}{3s}\sqrt{s\,f_f(s)}\,\tanh\left(\sqrt{s\,f_f(s)}\right)$ $f_f(s) = \frac{3\omega_f}{\lambda_{Ac,Ff}} + \frac{3\omega_m\lambda_{Ac,fm}}{s\omega_m\lambda_{Ac,Ff} + \lambda_{Ac,fm}\lambda_{Ac,Ff}}$
Triple-Porosity Mixed Flow (Model 3)	$f(s) = \omega_F + \frac{3\omega_f\lambda_{Ac,Ff} + \frac{\lambda_{Ac,Ff}\lambda_{Ac,fm}}{s}\sqrt{\frac{3s\omega_m}{\lambda_{Ac,fm}}}\tanh\left(\sqrt{\frac{3s\omega_m}{\lambda_{Ac,fm}}}\right)}{3\lambda_{Ac,Ff} + 3s\omega_f + \lambda_{Ac,fm}\sqrt{\frac{3s\omega_m}{\lambda_{Ac,fm}}}\tanh\left(\sqrt{\frac{3s\omega_m}{\lambda_{Ac,fm}}}\right)}$
Triple-Porosity Fully PSS (Model 4)	$f(s) = \omega_F + \frac{\lambda_{Ac,Ff}\left[\omega_m\lambda_{Ac,fm} + \omega_f\left(s\omega_m + \lambda_{Ac,fm}\right)\right]}{\left(\lambda_{Ac,Ff} + s\omega_f\right)\left(s\omega_m + \lambda_{Ac,fm}\right) + s\omega_m\lambda_{Ac,fm}}$

VITA

Name: Hasan Ali Alahmadi

Address: P.O. Box 13970
Saudi Aramco
Dhahran 31311
Saudi Arabia

Email Address: ahmadihas@hotmail.com

Education: B.Sc., Petroleum Engineering, King Fahd University of Petroleum & Minerals (KFUPM), Saudi Arabia, 2005

M.S., Petroleum Engineering, Texas A&M University, 2010